SLAC-PUB-8356
January, 2000

Particle Identification Methods in High Energy Physics[1]

J.Va'vra
Stanford Linear Accelerator Center, Stanford, CA 94309, USA

Abstract

This paper deals with two major particle identification methods: dE/dx and Cherenkov detection. In the first method, we systematically compare existing dE/dx data with various predictions available in the literature, such as the Particle Data group recommendation, and judge the overall consistency. To my knowledge, such comparison was not done yet in a published form for the gaseous detectors used in High-Energy physics. As far as the second method, there are two major Cherenkov light detection techniques: the threshold and the Ring imaging methods. We discuss the recent trend in these techniques.

I. INTRODUCTION

The dE/dx method predictive power relies on the detailed knowledge of dE/dx energy loss parameterization and its resolution. Given the two quantities, one can predict particle separation of two particles of mass m_1 and m_2 in terms of the number of sigma:

$$D = \frac{dE/dx(m_1) - dE/dx(m_2)}{\sigma(dE/dx(m_2))} \quad . \tag{1}$$

In this paper, to predict the dE/dx curve, I use the Particle Data Group [1] recommendation, which is based on the modified Bethe average energy loss model. The original Bethe theory from 1930 describes total energy loss [2], which is applicable to range measurements, but not to drift chambers. Neglecting the shell and other corrections, the restricted energy loss rate describing the energy deposited, which is applicable to the drift chamber measurements, is given by [1]:

$$\frac{dE}{dx} = -0.3071 \frac{Z}{A} \rho t \frac{z^2}{\beta^2} [\frac{1}{2} \ln \frac{2 m_e c^2 \beta^2 \gamma^2 E_{cut}}{I^2} - \frac{\beta^2}{2} - \frac{\delta}{2}] \quad , \tag{2}$$

where ρ, Z, A, and I are density, atomic number and mass, and the mean excitation energy in a given gas mixture [3], E_{cut} is a value, which is lower than the maximum energy and can be given to a free electron (in practice, as we will show, it is a tunable free parameter); and δ is the density function, describing the polarizabilty of the medium, which is calculated using the Sternheimer empirical formulas [3]:

$$\begin{aligned} &\delta = 0 && \text{for} \quad X = \ln\beta\gamma < X_0 \quad , \\ &\delta = 4.606(X - X_a) + \frac{4.606(X_a - X_0)}{(X_1 - X_0)^3}(X_1 - X)^3 && \text{for} \quad X_0 \le X < X_1 \quad , \\ &\delta = 4.606(X - X_a) && \text{for} \quad X > X_1 \quad . \end{aligned} \tag{3}$$

In this paper, I call this method the Bethe-Sternheimer parameterization. To my knowledge, there is no published reference describing how consistently this particular parameterization works in quantitative detail for the gaseous detectors, or what are the typical E_{cut} values obtained by various major measurements.

In more recent editions of the Particle Data Group data books [4], one can find a slightly different parameterization of the dE/dx formula:

$$\left.\frac{dE}{dx}\right|_{T<T_{cut}} = -0.3071 \frac{Z}{A} \rho t \frac{z^2}{\beta^2} [\frac{1}{2} \ln \frac{2 m_e c^2 \beta^2 \gamma^2 T_{upper}}{I^2} - \frac{\beta^2}{2}(1 + \frac{T_{upper}}{T_{max}}) - \frac{\delta}{2}] \quad , \tag{4}$$

where $T_{upper} = MIN(T_{cut}, T_{max})$, T_{cut} is a "tuned" maximum energy transfer and T_{max} is the maximum kinetic energy which can given to a free electron in a single collision. However, in all gaseous detector examples presented in this paper, $T_{cut} << T_{max}$, and, the equation 4 can be approximated with equation 2 in most of the kinematics region, except at extremely low energy.

---

[1] Invited talk at the 7-th International Conference on Instrumentation for Colliding Beam Physics, INSTR99, Hamamatsu, Japan, November 15-19, 1999. Work supported by Department of Energy contract DE-AC03-765SF00515.

In the literature, one can also find predictions based on Monte Carlo programs. The most frequently quoted work is due to Allison-Cobb [5], which is a widely adopted theoretical approach. Unfortunately, to date, no standard computing package is provided, to my knowledge. In addition, the photo-ionization cross-sections are not available for any gas. Therefore, in this paper, I use this model only if the prediction happens to exist, which is typically only for noble gases, such as argon or helium.

In the past, many have used the Landau formula to calculate the most probable energy loss [6]. Landau derived this formula in 1944, based on the Bethe's theory. It does not have a free parameter E_{cut}, which is available in the modified Bethe formula. This removes a possibility to "tune" the relativistic rise, resulting in disagreements with the data. The Landau formula has the form:

$$\frac{dE}{dx} = -0.153 \frac{Z}{A} \rho t \frac{1}{\beta^2} [\ln \frac{m_e c^2 \beta^2 \gamma^2 (0.153 \frac{Z}{A} \rho t)}{I^2} + 0.891 - \ln\beta^2 - \beta^2 - \delta] \quad . \tag{5}$$

Typically, the large experiments do not apply to the above models directly. Instead, they fit a parameter formula to the data. For example, Ronaldi and Blum [7] have used this particular 5-parameter formula (warning: not to be used at very low β):

$$\frac{dE}{dx} \Big/ \frac{dE}{dx}(\text{min}) = \frac{p_1}{\beta^{p_4}} \{ p_2 - \beta^{p_4} - \ln[p_3 + (\frac{1}{\beta\gamma})^{p_5}] \} \quad . \tag{6}$$

The dE/dx resolution, σ(dE/dx), is either obtained from the empirical dependence of the resolution on some parameter, for example, the electron density of the medium, or using the Allison-Cobb calculation (see Chapter 2.2.).

Chapter 3 discusses the Cherenkov technique. A basic difficulty of the Cherenkov technique is related to the small number of available photons. The number of produced Cherenkov photons dN_{foton} in the energy interval E to E+dE is calculated using Frank-Tamm equation:

$$\frac{dN_{foton}}{dE} = \frac{z^2 \alpha}{hc} L \sin^2 \theta_c = \frac{z^2 \alpha}{hc} L [1 - \frac{1}{(n(E)\beta)^2}] \quad . \tag{7}$$

A number of detected photoelectrons N_{pe} in RICH detectors is typically only 10-40, and this number is determined empirically from measurement of various detection efficiencies, mirror reflection, quantum efficiencies, etc. as follows:

$$N_{pe} = L \frac{z^2 \alpha}{hc} \int_{E_1}^{E_2} \prod_i \varepsilon_i(E) \sin^2 \theta_c(E) \, dE \quad , \tag{8}$$

where a product $\Pi\varepsilon_i$ is the empirically determined quantity. In this paper, to judge various RICH detector designs, I make my own estimate of N_{pe}. For the general Cherenkov particle identification math, I refer the reader, for example, to paper of P. Glaessel [8].

II. dE/dx TECHNIQUE

2.1. Energy Loss

Figures 1-6 compare data with dE/dx predictions based on the Bethe-Sternheimer formula, as published by the Particle Data Group, and the Landau-Sternheimer formula. In these two cases, the author performed both calculations for many gases at different pressure. The Allison-Cobb Monte Carlo prediction is shown only for argon gas only. The data were compiled from either large experiments [9] or tests [10]. Except in a few cases, the experiments provide only relative energy losses, which are normalized to dE/dx(min). It is very desirable that all future experiments provide absolute dE/dx values to test the models more fully.

Table 1: Relationship between variables E_{cut} and [dE/dx(min)]dx in several examples used in this paper (see Figs.1-6).

Gas	Pressure [bar]	Sample [cm]	dE/dx(min) [kV/cm]	[dE/dx(min)]dx [keV]	E_{cut} [keV]
90%Ar+10%CH_4 (Walenta)	1	2.3	1.45	3.34	1.3 ± 0.5
95%Ar+5%CH_4 (Lehraus)	1	4.0	1.45	5.96	1.5 ± 0.7
80%Ar+20%CH_4 (LBL TPC)	8.5	0.4	12.07	4.83	1.3 ± 0.5
88.2%Ar+9.8%CH_4+ 2%iC_4H_{10} (OPAL)	4	1.0	6.55	6.55	4.5 ± 1.5
90%Ar+5%CH_4+5%CO_2 (NA49)	1	3.8	1.68	6.38	6.0 ± 3.0
80%Ar+20%CO_2 (CRISIS)	1	1.6	2.49	3.98	1600 ± 1000

In all cases, the Landau-Sternheimer formula does not agree with the data, and there is no convenient free parameter available to correct this. Similarly, Figure 2 shows that the data are not quite reproducible by the Allison-Cobb prediction either. Combining the 1982 and 1978 data from Lehraus [10], we find a disagreement with the Allison-Cobb 1980 prediction at a ~3% level [5]. Such

disagreement is significant for the particle identification in the relativistic rise region. On the other hand, the Bethe-Sternheimer formula can be "tuned" using the variable E_{cut} to agree with the data within ~1% percent, except in the momentum region below 100-200MeV/c, where disagreements, as much as 5-10%, were found. Table 1 shows that variable E_{cut} is rather inconsistently related to a minimum energy loss dE = [dE/dx(min)]dx (this is especially apparent in case of the CRISIS experiment, which differs so much, that one may worry that it may be incorrect). This is probably because a value of E_{cut} is sensitive to systematic error in the measurement of the relativistic plateau, absolute calibrations, a method of truncation of large samples, or even possible errors in the Sternheimer density correction. In addition, because the E_{cut} variable appears in the logarithm of the equation (2), one needs a very precise data to define it well. Finally, the variable E_{cut} appears to be known only after the measurement is finished, and that does speak well for any theory.

2.2. Energy Loss resolution

Figures 7-9 compare the data with the FWHM dE/dx resolution for a single sample with predictions based on a simple power law fit. The Allison-Cobb Monte Carlo prediction is available only for argon and helium based gases (large open circles). The data were compiled from 23 large experiments [9] (black squares), and 86 tests [10] (all other symbols), covering many gases at different pressure and sample sizes. Figure 7 shows the result, i.e., the resolution on linear and log scales as a function of the variable $\zeta = 0.153(Z/A)\rho t/(I\beta^2)$, which is proportional to electron density of the medium (the variable ζ was introduced by Ermilova et al. [11]). A fit gives a dependence $FWHM(n=1) = 94.344*(\zeta)^{-0.3165}$ (for example, Allison, who did a similar fit to Walenta's data only, obtained $FWHM(n=1) = 81*(\zeta)^{-0.32}$ [5]). The Allison-Cobb Monte Carlo prediction of the resolution agrees reasonably well with the data, although it tends to be slightly optimistic. Figure 8 shows the resolution as a function of $x = \zeta$ * [dE/dx/dE/dx(min)], which is the same variable, but corrected for the relativistic rise. A fit gives the dependence $FWHM(n=1) = 97.448*(x)^{-0.31633}$. Figure 9 shows the resolution as a function of the variable y = N-ions* [dE/dx/dE/dx(min)], which is a number of primary ion pairs generated in a given sample, corrected for the relativistic rise. It is clear that this correlation is the worst. The relativistic rise correction improves the correlation only slightly. It is not entirely clear why the correlation with primary ions is so much worse. I have tried various literature sources for the number of primary ions (see Table 2), and none would improve the correlation. In fact, one can see that literature sources differ substantially for some gases.

Table 2: Number of primary ion pairs produced by minimum ionizing particles in 1cm sample at 1 bar and at 0°.

Gas	Zarubin [12]	Riecke Prepejchal [13]	Grupen's book [14]	Malamud [15]	Fehlman's fit to data [16]	My "blind tune"
H_2	4.7	4.7	5.2		1.45	4.7
He	3.3	6	5.9		2.9	12
Ne	10.9	24.1	12		31.9	24.1
Ar	24.8	24.1	29		26.1	24.1
Kr	33		22		46.4	
Xe	44.8	78.3	44		78.3	25
CH_4	24.8	26.6	16	26	14.5	26.6
C_2H_6	40.5	43.5		51	26.1	43.5
CO_2	33.6	36	34		31.9	65
C_3H_8	67.6	72.4		74	37.7	140
iC_4H_{10}	83.6	89.6	46	93	49.3	68
DME		66.2		62	37.7	

Figure 10(a) gives the hint at the explanation. It shows a very poor correlation between the above defined variables x and y, plotted for various gases, sample sizes, and gas pressures. Figure 10(b) shows that one can improve this correlation by "tweaking" the number of primary ions for He, Xe, CO_2, C_3H_8, and iC_4H_{10} gases (see Table 2), arbitrarily at this point. The improvement in the correlation may hint that either the numbers in the literature are not entirely correct, or the number of created primary ion pairs are influenced by the mixture, and one cannot simply add contributions from individual components. This suggests that to obtain the correct number of ion pairs for a given gas mixture, one may have to include also a constraint of obtaining the best possible correlation between x and y variables. Of course, we have neglected the saturation effect in our discussion of the primary ionization, which screens later arriving charge clusters even at very low gas gains [17]. This is certainly a problem at a practical level. However, the incorrect number of primary ions may be a dominant variable in this problem already at the theoretical level.

To get the resolution for n samples, which is needed in equation (1), one can use empirical scaling $\sigma(n) \sim \sigma(n=1)*n^{-0.43}$ [18].

2.3. dE/dx Particle Identification example

Figure 11 shows an example of the impressive dE/dx performance in the NA-49 experiment [9]. Two very large TPCs, filled with 90%Ar+5%CH_4+5%CO_2 at 1 bar, measure tracks up to 7 m long with a sample length of 3.8 cm. Up to 1500 tracks are recorded in one Pb-Pb collision. There is no Cherenkov detector that can compete with this performance. As Lehraus [10] showed empirically a long time ago, the price for the best performance dE/dx detector is not small: it is very long and operating at 1 bar. For the general dE/dx systematics, I refer the reader, for example, to paper of M. Hauschild [18].

III. CHERENKOV RING IMAGING TECHNIQUE

RICH detectors, which were or will be used, for physics, can be categorized into three groups. Detectors such as OMEGA, DELPHI RICH, SLD CRID, CERES, JETSET, CAPRICE, etc. belong to the first generation of detectors. ALICE, HADES and CLEO belong to the second generation, and generation HERA-B, LHC-b, HERMES and DIRC fall into the third generation. The 1-st generation was designed with typically 8-16 photoelectrons per ring, the 2-nd increased this number to 18-24, and the 3-rd has 30-60 (the largest number belongs to DIRC). We see a clear trend to improve the robustness of the RICH detectors by increasing the number of photoelectrons per ring.

3.1. Basic parameters of RICH detectors

Figure 12 shows quantum efficiencies and some of the critical transmission edges defining the bandwidth acceptance in some RICH detectors. Over the years there was a steady push to develop the RICH detectors operating in the visible wavelength region, mainly to avoid the large chromatic effects (see Fig.13 and Ref.19) and other operational complexities experienced in the far UV region. For example, HRS experiment at PEP-I was the first large detector to use a benzene molecule, which needs a far UV operation of photon energies above ~9eV. This is a very difficult region to operate, mainly from point of view of maintaining purity of materials, and as a result, the HRS detector achieved only 2-3 photoelectrons. A major progress occurred when D. Anderson [20] discovered a possibility to use a TMAE molecule, which photo-ionizes between 5.5 and 7.5eV, and allows the use of quartz windows. A TEA molecule was neglected for a long time, because its quantum efficiency is lower than that of TMAE, and because it still requires relatively hard photons to photo-ionize it (between 7.5 and 9eV). The first experiment to use it was E-605 at Fermi lab [21]. TEA was revived recently, thanks to work of Sequinot et al. [22], which was followed by work of the CLEO group – see chapter 3.3. Both CsI and TEA photo-cathodes allow a construction of thin photo-detectors with small dE/dx deposits. Lower quantum efficiency of TEA or CsI is usually offset by a design eliminating one extra window. However, as I said, there is a clear trend towards the operation in the visible wavelength region, which is made possible by the general acceptance of the PMTs as fast photon detectors capable of imaging at high luminosity accelerators.

3.2. Lessons from the first generation RICH detectors

RICH detectors, such as DELPHI [23], CRID [24], and OMEGA [25], pioneered the path for acceptance of the RICH technique. The main accomplishment was to show that it was possible to detect single photoelectrons on a very large scale using gaseous detectors, which was not obvious in the beginning. Other lessons that were learned [24]: (a) it was possible to maintain the purity of a large UV system for many years, (b) it was possible to purify gases, including TMAE, to drift single electrons over a 1 meter distance, (c) TMAE is not as chemically aggressive as originally feared (detector surfaces were found in a very good shape), (d) the distillation is the preferred cleaning method for filtration, (e) TPC-based detectors are easily maintainable (for example, it took ~45 minutes to replace a CRID detector once the TMAE was purged).

As in any pioneering effort, errors were made. For example, TPC detectors were made too thick creating large dE/dx deposits and electronics cross-talk. The adopted shaping times were too short requiring large gas gains, which caused avalanche photons in TMAE, and therefore detectors required building "barricade electrodes" around the anode wires. The experiments, based on the initial "excessive worries" about TMAE, were made rather complex, which discouraged followers. Finally, the TMAE wire aging [26,27] was found to be real at the end, and effectively prevented TMAE to be used in high luminosity applications such as LHC-b, HERA-B, or B-factories.

However, the TMAE-based detectors went a long distance since the beginning. For example, when T. Francke (CAPRICE [28]) was asked why he flies the TMAE-based, rather than the CsI-based, RICH detector in a sophisticated balloon experiment in remote parts of Northern Canada, his answer was: "It is easier to maintain it there". In principle, TMAE still could be used for low rate applications in the future, for example, for particle identification up to 40-50GeV/c, which requires a gaseous radiator. Its main advantage: continuously refreshing, high quantum efficiency, allows the use of quartz, and avoids operation in the far UV region.

3.3. The second generation RICH detectors

Second generation devices accomplished very important transformation. They traded high gas gain ($2\text{-}5\times10^5$), short charge integration constant (10-100ns) and drift time measurement, for small gas gain ($\sim5\times10^4$), long charge integration constant (600-1000ns), low noise electronics (< 500 e^- rms), and geometrical pixelization. In addition, the detectors are thin. In principle, all three photo-cathodes, i.e., TMAE, TEA, and CsI, can be used in this approach, although in the case of TMAE it means a hot TMAE bubbler temperature (~35°C), which is rather impractical. Detector operations at very low total gas gain results in an exponential pulse height spectrum. The only way to have good single electron detection efficiency (>90%) under such conditions is to have very low noise electronics (~500 e^- rms). It is important to say that the gaseous detectors benefited from developments of the high-density silicon detector electronics.

However, one should immediately add that the above recipe is not adequate for the very high rate applications of RICH detectors at LHC or HERA-B, where the required short shaping times cause a high gas gain operation, which results in the anode wire aging and cathode dark currents. The photo-cathode materials, such as TMAE or TEA, are good insulators, especially after the purification procedure removes water. Therefore photon detectors, which use such photosensitive materials, are sensitive to the Malter effect [29,30] at high rates, which can manifests itself not only as a steady dark current, but also as sporadic bursts of charge [31]. Similar problems apply for detectors with the CsI-based photo-cathode as demonstrated by many LHC or HERA-B

tests [32,33,34]. Currently there is no "successful experiment-proven" working solution for the RICH gaseous detectors in the LHC or HERA-B in the highest rate regions, which require shortest integration times, although R&D studies are performed presently on various novel gaseous detectors such as MICROMEGAS [35], GEM [36,37], or CAPILLARY TUBES [38]. However, one may argue that a high gain operation forced by the short integration constant may bring gaseous detectors close to the sparking limit, resulting in possible long-term degradation.

Examples of the second generation of RICH detectors, which are to be used for the moderate rates, are ALICE [39] (Figs.14-15), HADES [40] and CLEO [41] (Figs.16-18). Test beam results, in terms of N_0 and number of photoelectrons per ring, are shown in Table 3. ALICE and HADES are the first RICH detectors, which adopted the CsI solid photocathode on a very large scale. They solved a number of R&D puzzles, such as how to produce good quality large area photocathodes, or how to develop a low noise pad readout system. ALICE is using C_6F_{14} liquid radiator; benefiting from the DELPHI RICH experience. On the other hand, CLEO has adopted a novel method to solve the problem of planar solid radiators that light does not escape for perpendicular tracks if the refraction index is larger than $\sqrt{2}$. This was solved by creating precise grooves in the LiF radiator in the central region of the detector (Fig. 16(a)). According to my estimate, there is still ~50% light photon loss at 0° incidence, but this solution is more attractive than tilting the planar solid radiator, and operationally, the solid radiator promises stable, long-term operation. The grooves cause a complicated ring image pattern (Fig. 16(b)), however, as Fig.18 indicates, the measured angular resolution in the test beam is as expected. CLEO has adopted the TEA photocathode, which allows an ambient temperature operation, a short photon absorption length, and thus, the detector can be thin. Furthermore, TEA is a better quencher than TMAE, and it has a lower rate of wire aging compared to TMAE [42] (see Fig.19), although the Malter current can also be excited. As the CLEO will push luminosity well beyond $10^{34}cm^{-2}sec^{-1}$, it will be an interesting to check this, although, low gas gain operation will help.

3.4. The third generation RICH detectors

Third generation devices further reduced the charge integration constant to 10-20ns, which is necessary to accommodate the high rates of new machines. So far, all the devices in this group abandoned the gaseous photon detectors in favor of vacuum operated PMTs or HPDs operating with bi-alkali photocathodes, which are sensitive to photons in the visible wavelength region. All RICH detector systems in this group are designed for at least 30 photoelectrons per ring, which is a factor of 2-3 higher compared to the first generation RICH detectors. Examples of the third generation RICH detectors are HERA-B [43] (Figs. 20-21), DIRC [44] (Figs. 22-23), and LHC-b [45] (Figs. 24). The HERA-B RICH has suffered from no tracking in the initial period, however, it is already clear that it performs well in very high background conditions. The detectors use Hamamatsu fast multi-anode PMTs (R5900-000M16 and R5900-03-M4, with 4x4 and 9x9 mm^2 anode pads respectively). They replaced originally proposed TMAE-based gaseous detectors, which suffer from the wire aging effect [46]. The PMTs are equipped with de-magnifying optics (Fig. 20) with rather large transmission losses of ~35% at 350nm (Fig. 21). In addition, the multi-anode PMT photoelectron transfer efficiency is only 75% at present [47]. It is interesting to point out that if CRID, with its ~45 cm long gas radiator system, would have used the existing HERA-B detection system, it would have measured only ~5 photoelectrons per ring instead of 9-10, i.e., HERA-B RICH benefits from a very long 2.7 m radiator path. Or, to put differently, a TMAE-based detector is rather efficient.

DIRC is the new BaBar detector recently completed at SLAC, which is designed to perform the πK-separation up to ~4GeV/c. It has been recently successfully commissioned and already started to produce physics. Its main attractions are large number of photoelectrons, speed, stability and radiation hardness. It uses 1.7cm thick radiation resistant synthetic quartz radiator. Produced photons are propagated along the quartz bar via internal reflection all the way out of the magnet, where they are imaged on a plane of ~11,000 PMTs. A typical photon makes ~200 internal reflections on average and travels 2-to-7 meters along the quartz bar. The DIRC projecting geometry causes ambiguities in number of possible solutions (2-16), many of which, are eliminated by applying geometrical and timing cuts. The present DIRC has ~1.8ns timing resolution per photon hit. This still leaves some ambiguities, which contribute together with other sources, such as the δ-rays or scintillation or bar chips, to a combinatorial background, that is slightly larger (Fig. 22(a)) than the typical non-projecting RICH detectors presented in this paper. If a future DIRC would attempt to run with a time resolution of 200ps, it would eliminate ambiguities completely. Examples of various efficiencies in the DIRC are shown in Fig. 23. One can see that the internal reflection coefficient's wavelength dependence can be for some track orientations a non-negligible chromatic correction in DIRC, depending on number of bounces. The present DIRC, as implemented by BaBar, uses water as a coupling medium between the quartz bars and the PMTs. This creates complications, such as difficult access, possible leaks, interaction of clean water with various materials, source of background from few MeV photons, etc. The present DIRC background is still small at luminosity of $1\text{-}3x10^{33}cm^{-1}sec^{-1}$. However, for future planned upgrades to increase the luminosity by a factor of 10, DIRC may need additional shielding. There is an active, long-term R&D effort to develop a DIRC detector without the need to penetrate the magnet iron, and without the water coupling, i.e., which would allow for operation in a magnetic field. Presently, only Monte Carlo studies and some very simple initial tests were performed, for example, with the AVALANCHE DIODE ARRAYS [48,49,50,51,52]. There is still a long way to go though, but the trend seems to be clear. Whatever the choice, I believe, the future DIRC should aim for a sub-nanosecond timing resolution.

LHC-b has two RICH detectors employing three radiators: aerogel, C_4F_{10}, and CF_4 gases. A slight CF_4 gas scintillation [53] is quite acceptable. The CERN developed HPD photon detector has 2048 silicon elements, charge gain of $4x10^4$ at 20kV, efficiency of 94%, and very good multi-hit performance. However, so far, a "non-LHC" shaping constant of 1.3μs was used. Figure 24 shows various efficiencies for a 5cm thick aerogel radiator. It shows a fraction of non-scattered photons due to the Rayleigh scattering, which is tolerable in the visible wavelength region only. The expected performance is shown in Table 3. The CERN

made HPD photon detector [45] is in competition with two other photon detector solutions presently: a 64-channel multi-anode PMT, manufactured by Hamamatsu, and a 2048-pixel HPD, manufactured by DEP [54].

Table 3: Performance of second and third generation RICH detectors. The author's prediction is based on a spreadsheet type of calculation. For a case of LHC-b, author assumed the CERN developed HPD detector [45].

RICH	Condition	N_0 [cm^{-1}] (author)	Npe (author)	Npe (data)
ALICE	$\Theta_{inc} = 0°$, test beam data	44	17	23
CLEO	$\Theta_{inc} = 0°$, saw-tooth radiator	34	18-19	19
HERA-B	C_4H_{10}	45	32	31
DIRC	$\Theta_{inc} = 0°$, middle section	36	32	33
LHC-b	Aerogel (RICH1a)	58	16	-
LHC-b	C_4H_{10} (RICH1b)	181	46	-
LHC-b	CF_4 (RICH2)	174	29	-

IV. CHERENKOV THRESHOLD TECHNIQUE

The performance of a threshold detector is not as good as that of a RICH detector, in terms of the ultimate performance. However, a threshold detector is simpler, and that may be valuable in the long run. In the past, the aerogel materials used were not stable, mainly because they were attacked by water. During the past several years, there was a tremendous effort to develop new aerogel radiators, which are more stable, water resistant, and have lower refraction index. After the pioneering effort of Hrubesh to develop a two-step method to produce very low refraction index materials in the range of 1.007-1.03 [55], the KEK Belle group developed the first water resistant version [56].

Figure 25 shows the particle identification principle with a threshold aerogel detector. It is clear that one desires to have the refraction index as low as possible in order to obtain a π/K separation at as high momentum as possible. The KEK Belle detector module contains five aerogel tiles and is equipped with two Hamamatsu wire mesh PMTs R6681, R6682, or R6683, which can operate in magnetic fields of 1.5T. The PMTs are coupled to silica aerogel tiles of n =1.02, 1.015 and 1.01, respectively. Figure 26 shows a clear capability of particle identification of this system.

The aerogel in the KEDR detector, which was built in Novosibirsk, is even more transparent, although not water-resistant. Therefore it has to be kept in a gas tight enclosure. Its read out is a combination of wavelength shifter and a PMT equipped with a micro-channel plate (MCP), which can operate in a large magnetic field [57]. This is the first successful application of this type of detector.

V. CONCLUSIONS

The Bethe-Sternheimer dE/dx formula can be tuned to reproduce experimental data within ~1%, if the variable E_{cut} is chosen appropriately. The exception is the low momentum region below 100-200MeV/c. However, I do not see a consistent correlation between the E_{cut} variable and minimum energy loss, which does not allow to predict this parameter before the data is known. This may be either due to experimental errors, method of truncation, or inconsistencies in the Sternheimer parameterization of the density correction. The Landau-Sternheimer formula does not reproduce experimental data. The Allison-Cobb Monte Carlo reproduces the dE/dx relativistic rise plateau of the argon-based gases with no better accuracy than ~3%; the low momentum region was not tested. We find that the dE/dx resolution correlates well with the electron density of the medium. However, the correlation with a number of primary ions is still poor. The paper suggests that this could be explained by incorrect values of the number of ions for some gases. The Allison-Cobb Monte Carlo predicts reasonably well the resolution for helium based gases, although it tends to be on slightly optimistic side.

The performance of the threshold aerogel Cherenkov detectors, such as Belle or KEDR, has been as expected, which indicates a tremendous progress the aerogel radiator made since its early days.

The first generation RICH detectors, such as the CRID, DELPHI, or OMEGA, convinced many skeptics in the high-energy physics community that the RICH concept can be implemented to yield useful physics. The second generation of RICH detectors, such as ALICE, HADES and CLEO, learned from some of the early mistakes of the gaseous detectors and traded drift time for the pad readout, while running a low gas gain with a long shaping time. The third generation of RICH detectors, such as HERA-B, DIRC, or LHC-b, traded the gaseous detectors for the vacuum based PMTs or HPDs. This was done to cope with high rates, aging problems, and to operate the device in the visible wavelength region to reduce chromatic errors, and to simplify general operation.

However, the clock is not stopping, and effort to develop the fast radiation hard detectors continues. There is, presently, a very active R&D effort developing photon detectors based on solid state detectors (AVALANCHE DIODE ARRAYS), or vacuum-based detectors (a combination of PMT and MCP, or HPDs), or new concepts of the gaseous detectors (MICROMEGAS, GEM, CAPILLARY TUBES). Whatever the choice of the photo-detector, the future DIRC detectors should push a sub-nanosecond timing resolution to reduce the background and the reconstruction ambiguities.

ACKNOWLEDGEMENTS

I would like to thank Ch. Joram, A. Di Mauro, P. Krizan and Ch. Yeche for their willingness to answer some questions. I am also obliged to thank to W. Donwoodie and Prof. M. Regler for useful comments on the dE/dx topic.

REFERENCES

[1] J.J. Hernandez et al., Review of Particle Properties, Phys. Lett. 239 (1990) 1;
[2] N. Bohr, Phil. Mag., 25 (1913) 10; H. Bethe, Ann.Physik, 5 (1930) 325;
H. Bethe, Zeits. Fur Physik, 76 (1932) 293;
C. Moller, Ann. Der Physik, 14 (1932) 531;
L. Livingston and H. Bethe, Rev. Mod. Phys. 9 (1937) 245.
[3] E. Fermi, Phys. Rev., 57 (1940) 485;
R.M. Sternheimer, M.J. Berger and S.M. Seltzer, Atomic Data and Nuclear Data Tables 30 (1984) 261-271.
[4] C. Caso et al., European Physics Journal C 3, 1-794 (1998).
[5] W.W.M. Allison and J.H. Cobb, Ann.Rev.Part.Sci., 30 (1980) 253.
[6] L. Landau, "On the energy loss of fast particles by ionization," J. Phys., S (1944) 201.
[7] L. Ronaldi and W. Blum,"Particle Detection with Drift Chambers," Springer-Verlag, 1994.
[8] P. Glaessel, Nucl. Instr. Meth., A433 (1999) 17.
[9] dE/dx LARGE EXPERIMENTS:
ARGUS: H. Albrecht et al., Nucl. Instr. Meth.,A275 (1989) 1;
ALEPH: D. Buskulic et al., Nucl. Instr. Meth., A360 (1995) 481;
OPAL: M. Hauschild et al., CERN-PPE/91-130, Aug. 21, 1991;
DELPHI: Delphi Collab., Nucl. Instr. Meth., A303 (1991) 233;
LBL TPC: C. Caso et al., European Phys. Journal C, 31-794 (1998);
NA49: B. Lasiuk, Nucl. Instr. Meth., A409 (1998) 402;
CLEOI: R. Ehrlich et al., CLNS-80/459, June 1980;
CLEOII: Y. Kubota et al., Nucl. Instr. Meth., A320 (1992) 66;
JADE: H. Drumm et al., Nucl. Instr. Methods, 176 (1980) 333;
MARKII: A. Boyarski et al., Nucl. Instr. Meth., A283 (1989) 617;
OBELIX: F. Balestra et al., Nucl. Instr. Meth., A323 (1992) 523;
TOPAZ: M. Iwasaki et al., Nucl. Instr. Meth., A365 (1995) 143;
BELLE: S. Uno, Nucl. Instr. Meth., A379 (1996) 421;
KLOE: A. Andryakov et al., Nucl. Instr. Meth., A409 (1998) 390;
CRISIS: W.S. Toothacker et al., Nucl. Instr. Meth., A273 (1988) 97;
CRYSTAL BARREL: A. Abele et al., Phys.Rev. D, 57 (1998) 3860.
[10] dE/dx TESTS:
I. Lehraus et al., Nucl. Instr. Meth., 196 (1982) 361.
I. Lehraus et al., Nucl. Instr. Meth., 153 (1978) 347.
A. H. Walenta et al., Nucl. Instr. Meth., 161 (1979) 45;
A. H. Walenta, BNL report 28328, 1980;
A.P. Onuchin and V. I. Telnov, Nucl. Instr. Meth., 120 (1974) 365;
A. Yadigaroglu et al., Nucl. Instr. Meth., A323 (1992) 322;
I. Lehraus et al., CERN/EF/BEAM 80-5, 1980;
S. M. Playfer et al., Nucl. Instr. Meth., A315 (1992) 494;
J. Va'vra et al., Nucl. Instr. Meth., 203 (1982) 109.
[11] V. C. Ermilova, L.P. Kotenko and G.I. Merzon, Nucl. Instr. Meth., 145 (1977) 555.
[12] A. V. Zarubin, Nucl. Instr. Meth., A283 (1989) 409.
[13] F. F. Riecke and W.Prepejchal, Physical Rev. A, 6 (1972) 1507.
[14] C. Grupen, "Particle Detectors," Cambridge University Press, 1996.
[15] A. Pansky et al., Nucl. Instr. Meth., A323 (1992) 294.
[16] J. Fehlmann, ETH Zurich Ph.D. Thesis, 1980.
[17] J. Va'vra, Nucl. Instr. Meth., 225 (1984) 13.
[18] M. Hauschild, Nucl. Instr. Meth., A379 (1996) 436.
[19] J. Sequinot and T. Ypsilantis, Nucl. Instr. Meth., A343 (1994) 30.
[20] D. Anderson, IEEE Trans. Nucl. Sci., NS-28 (1981) 842.
[21] G. Countrakon et al., Nucl. Instr. Meth., A205 (1983) 403;
G. Charpak et al., Nucl. Instr. Meth., A1643 (1979) 419.
[22] R.Arnold et al., Nucl. Instr. Meth., A314 (1992) 465,
J.-L. Guyonnet et al., Nucl. Instr. Meth., A343 (1994) 178,
J. Sequinot et al., Nucl. Instr. Meth., A350 (1994) 430.
[23] E. Albrecht et al., Nucl. Instr. Meth., A433 (1999) 47.

[24] J. Va'vra, Nucl. Instr. Meth., A433 (1999) 59;
K. Abe et al., Nucl. Instr. Meth., A343 (1994) 74.
[25] U. Muller et al., Nucl. Instr. Meth., A433 (1999) 71.
[26] J. Va'vra, IEEE Trans.Nucl.Sci. NS-35, 1 (1987) 487.
[27] C. Woody, IEEE Trans. Nucl. Sci. NS-35, 1 (1988) 493.
[28] T. Francke et al., Nucl. Instr. Meth., A433 (1999) 87.
[29] L. Malter, Phys. Rev. 50 (1936).
[30] Guentherschultze, Z. Phys. 86 (1933) 778.
[31] J. Va'vra, Nucl. Instr. Meth., A367 (1995) 353.
[32] J. Seguinot et al., Nucl. Instr. Meth., A371 (1996) 64-78.
[33] P. Krizan et al., Nucl. Instr. Meth., A371 (1996) 151;
P. Krizan et al., Nucl. Instr. Meth., A387 (1997) 146.
[34] J. Va'vra et al., Nucl. Instr. Meth., A387 (1997) 154.
[35] I. Giomataris, SLAC-J-ICFA-19, Decmber 1999, (http://www.slac.stanford.edu/pubs/icfa/).
[36] R. Bouclier et al., SLAC-J-ICFA-13, December 1996, (http://www.slac.stanford.edu/pubs/icfa/);
S. Bachmann et al., Nucl. Instr. Meth., A433 (1999) 464.
[37] G. Garty et al., Nucl. Instr. Meth., A433 (1999) 476.
[38] V. Peskov et al., Nucl. Instr. Meth., A433 (1999) 492.
[39] F. Piuz et al., Nucl. Instr. Meth., A433 (1999) 178;
ALICE Technical Proposal, CERN/LHCC 98-19, 1998.
[40] K. Zeitelhack et al., Nucl. Instr. Meth., A433 (1999) 201.
[41] R. J. Mountain et al., Nucl. Instr. Meth., A433 (1999) 77;
M. Artuso et al., CBX 99-28, June 1999.
[42] J. Va'vra, Nucl. Instr. Meth., A433 (1997) 183.
[43] S. Korpar et al., Nucl. Instr. Meth., A433 (1999) 128;
D. Skrk, Ph.D. Thesis, Ljubljana University, 1999;
P.Krizan, ICFA Bulletin, SLAC-J-ICFA-19, December 1999, (http://www.slac.stanford.edu/pubs/icfa/).
[44] B. N. Ratcliff, SLAC-PUB-5946, 1992;
B. N. Ratcliff, SLAC-PUB-6047, 1993;
P. Coyle, Nucl. Instr. Meth., A343 (1994) 292;
The BaBar Tech. Design Report, SLAC-REP-950457, 1995;
D. Aston et al., IEEE Trans. Nucl. Sci. 42 (1995) 534;
H. Staengle et al Nucl. Instr. Meth., A397 (1997) 261;
I. Adam et al., IEEE Trans. Nucl. Sci. 45 (1998) 450;
J. Schwiening et al., IEEE Trans. Nucl. Sci. 42 (1998) 657;
J. Va'vra, "From CRID to DIRC", SLAC-PUB-7948, 1998;
B. N. Ratcliff and S. Spanier, Nucl. Instr. Meth., A433 (1999) 456;
A. Hoecker, Beauty 1999 Conf., Bled, Slovenia, LAL 99-56, Sept. 1999;
S. Korpar et al., Nucl. Instr. Meth., A433 (1999) 121;
S. Spanier et al., to be published in IEEE Trans. Nucl. Sci., Seattle, Washington, U.S.A., October 25, 1999.
[45] A. Bream et al., Nucl. Instr. Meth., A433 (1999) 153;
A. Bream, ICFA Bulletin, SLAC-J-ICFA-18, July 1999, (http://www.slac.stanford.edu/pubs/icfa/).
[46] J. Pyrlik, Nucl. Instr. Meth., A433 (1999) 92.
[47] Hamamatsu internal report, unpublished.
[48] T. Kamae et al., Nucl. Instr. Meth., A382 (1996) 430.
[49] M. Akatsu et al., DPNU-99-08, March 9, 1999.
T. Ohshima, a talk at this conference, INSTR99, Hamamatsu, Japan, November 15, 1999.
[50] R.J. Wilson, Nucl. Instr. Meth., A433 (1999) 487.
[51] Visible Light Photon Counters (VLPC) by Rockwell Int. Corp., see also M. Atac, Nucl. Instr. Meth., A314 (1992) 56.
[52] D. Lincoln, A talk at this conference, INSTR99, Hamamatsu, Japan, November 15, 1999. He described a use of the VLPC counters for the D0 experiment at Fermi lab. The device has 80% Q.E. at 540nm at cryogenic temperatures, a gain of 25000-50000 and can operate at single-photoelectron rates of 40MHz.
[53] A. Pansky et al., Nucl. Instr. Meth., A354 (1995) 262.
[54] E. Albrecht et al., Nucl. Instr. Meth., A433 (1999) 159.
[55] T. M. Tilotson and L. W. Hrubesh, J. Non-Cryst.Solids 145 (1992) 44.
[56] T. Sumiyoshi et al., Nucl. Instr. Meth., A433 (1999) 385;
T. Sumiyoshu, ICFA Bulletin, SLAC-J-ICFA-18, July 1999, (http://www.slac.stanford.edu/pubs/icfa/).
[57] A.P. Onuchin, A talk at this conference, INSTR99, Hamamatsu, Japan, November 15, 1999.
[58] Author fitted the water refraction index data obtained from N.I.Koshkin, M.G. Shirkevich, Handbook of Elementary Physics, p. 250, Mir Publishers, Moscow, Translation from Russian by G.Leib.

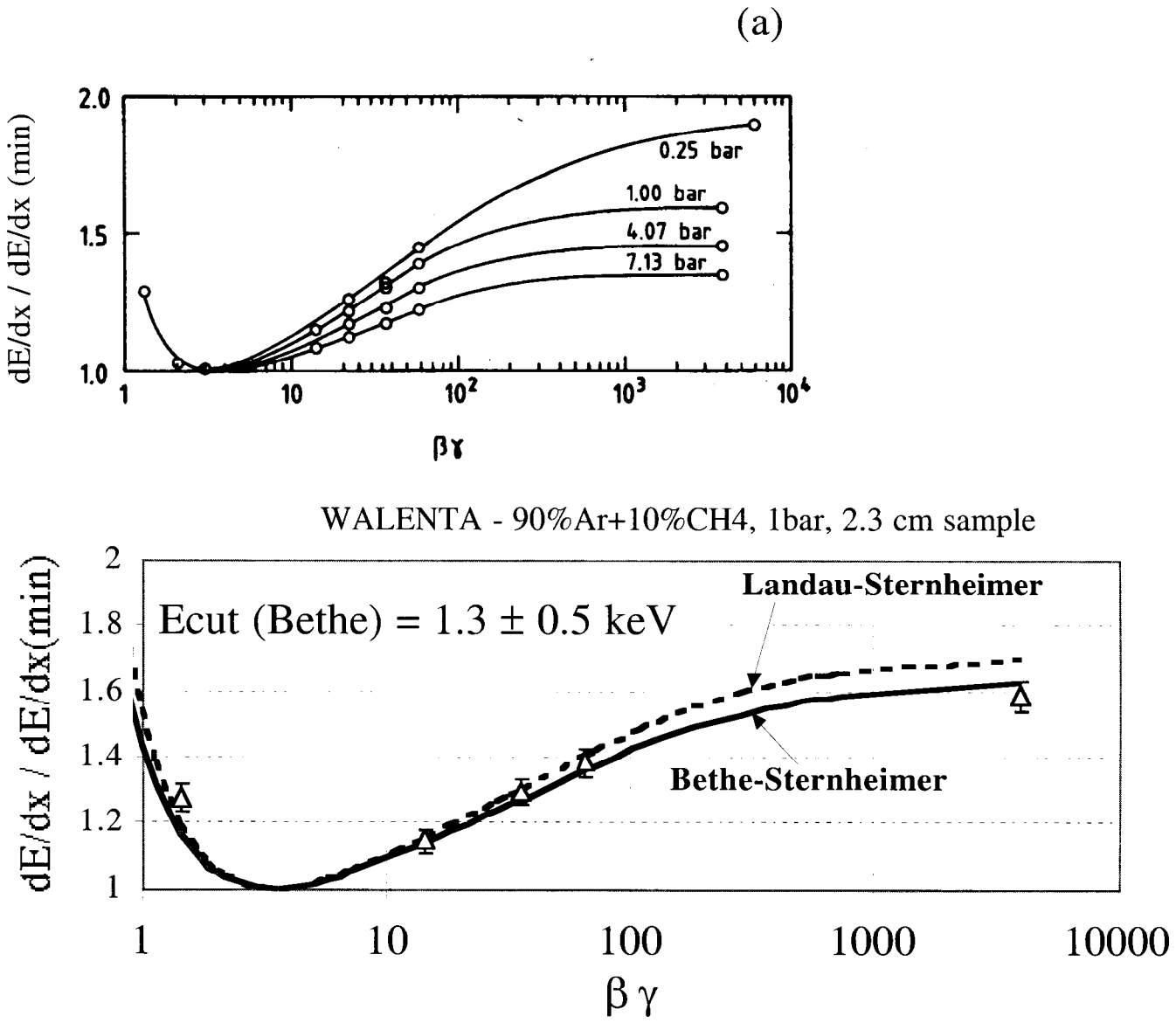

Figure 1: (a) Walenta's relative dE/dx measurement [10], (b) Predictions generated by the author for data taken at 1 bar pressure.

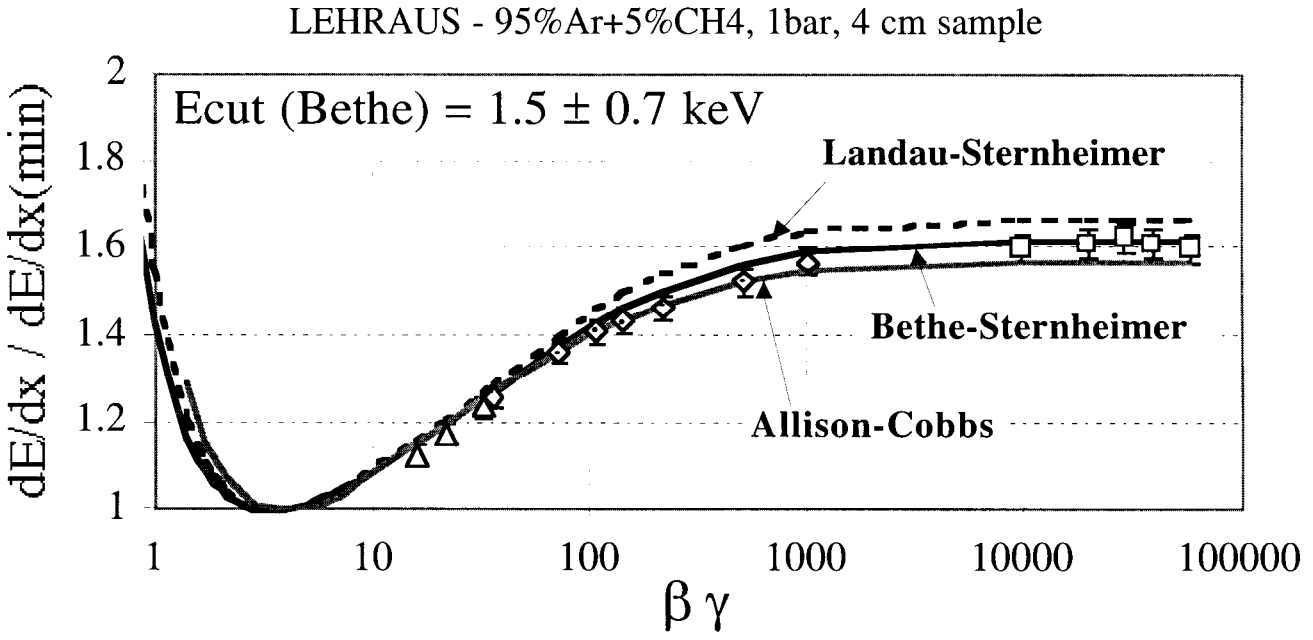

Figure 2: Lehraus's relative dE/dx measurement from 1982 [10]. Predictions generated by the author, except for predictions of Allison-Cobb [5].

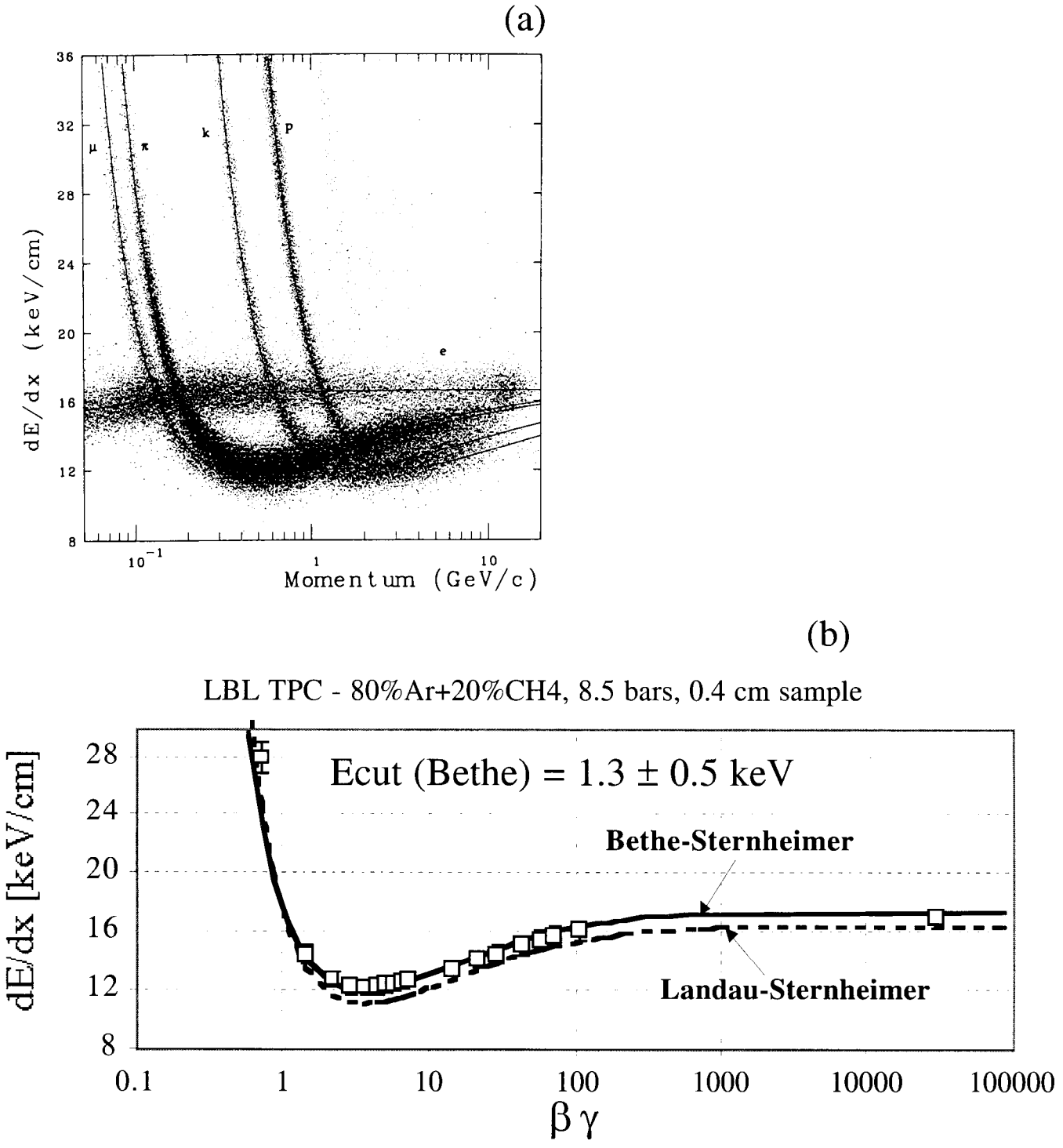

Figure 3: (a) LBL TPC absolute dE/dx measurement [9], (b) Predictions generated by the author and compared to their pion data.

(a)

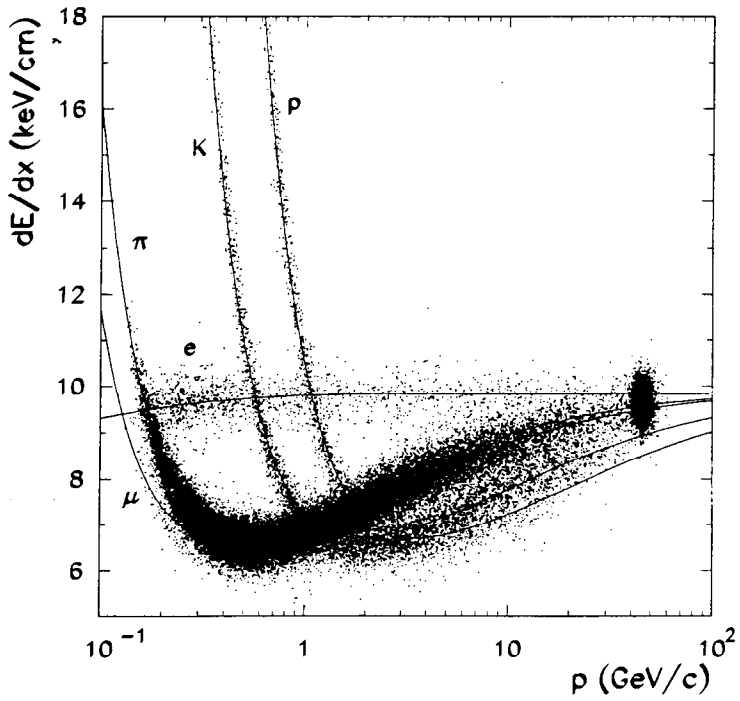

(b)

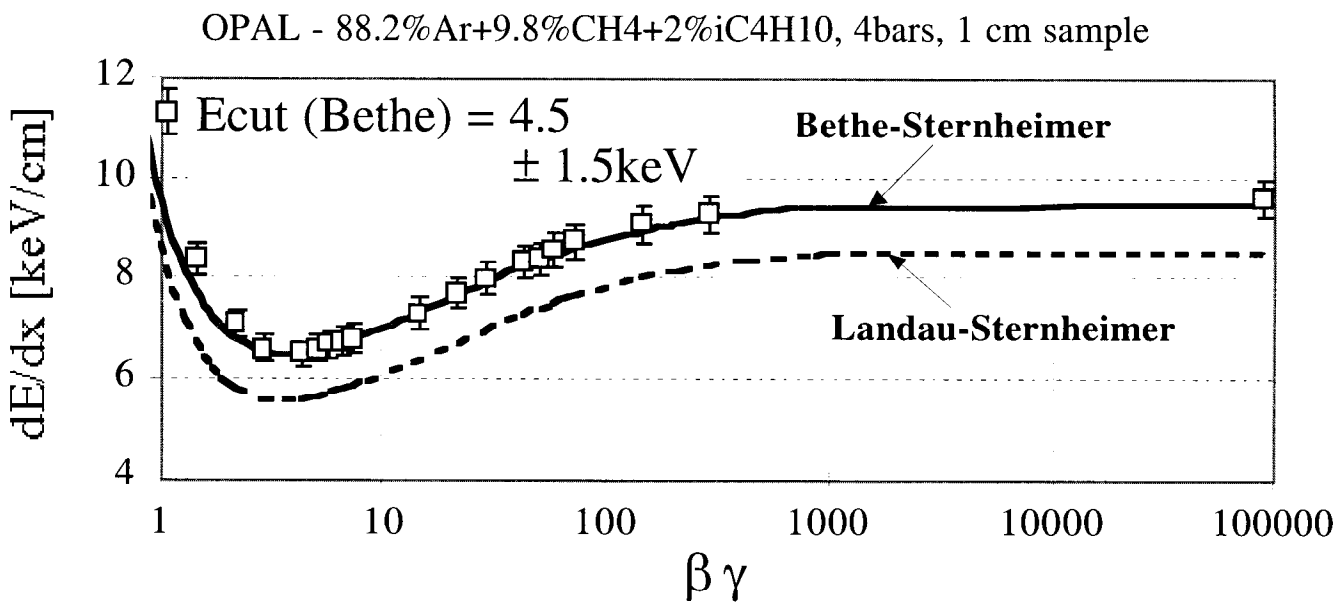

Figure 4: (a) OPAL absolute dE/dx measurement [9]. (b) Predictions generated by the author, which were compared to their pion data.

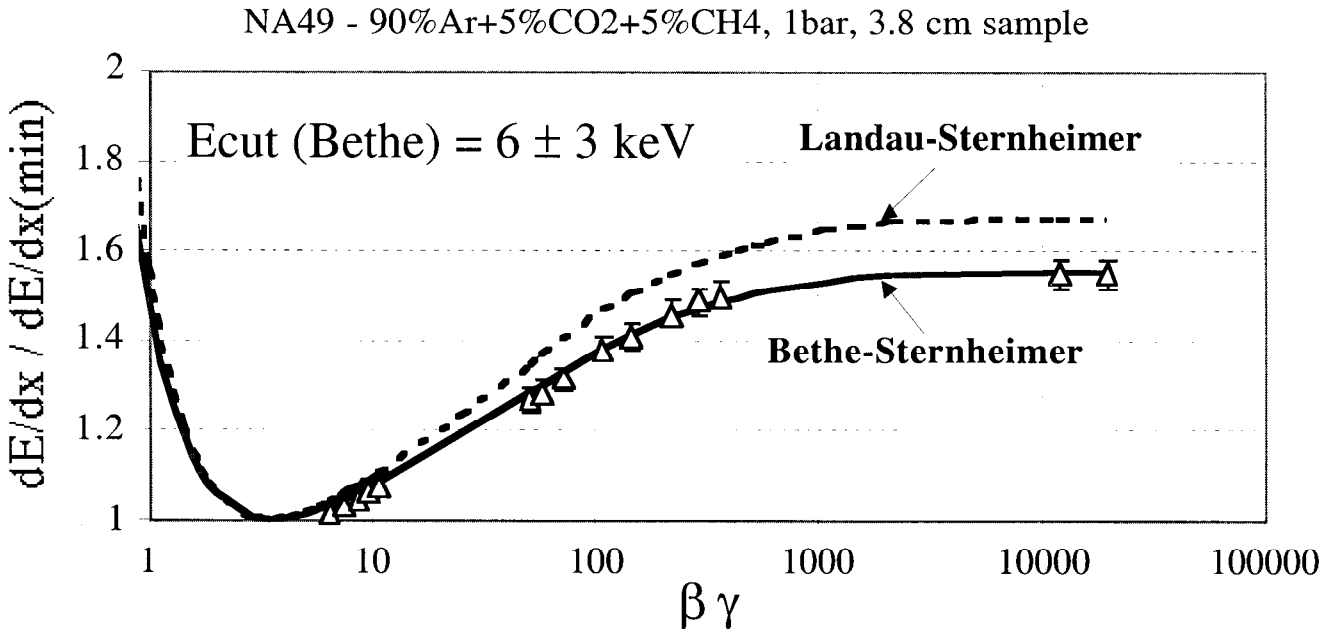

Figure 5: NA49 relative dE/dx measurement [9]. Predictions generated by the author.

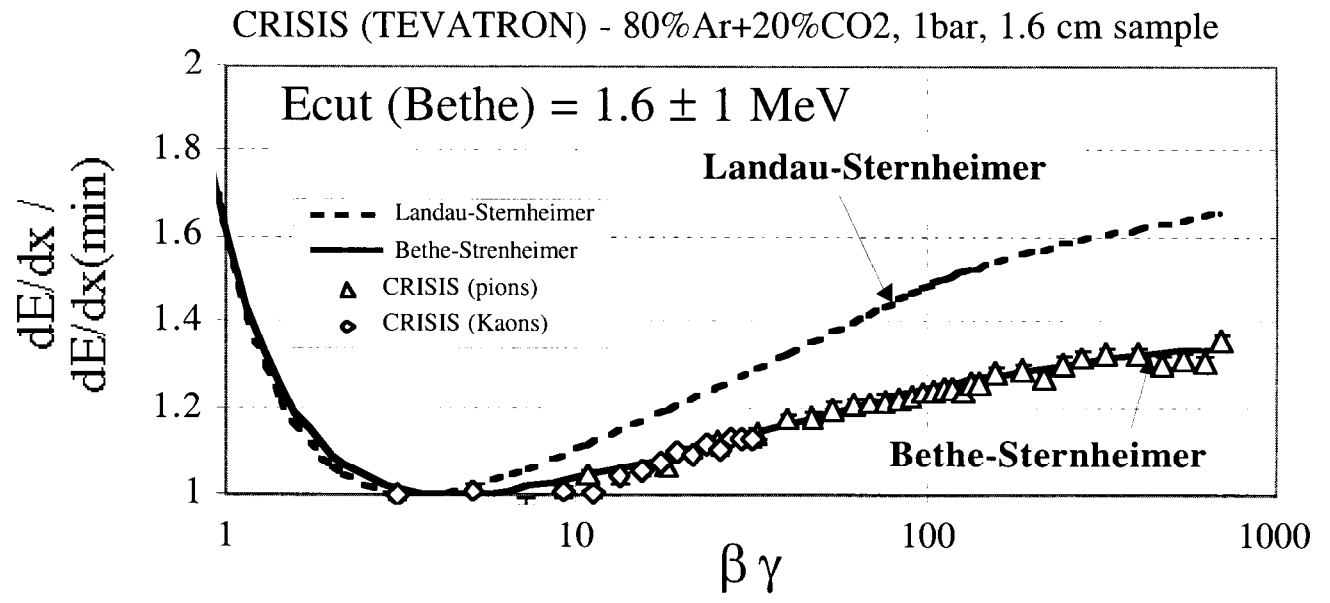

Figure 6: CRISIS relative dE/dx measurement [9]. Prediction generated by the author. A very large E_{cut} value needed.

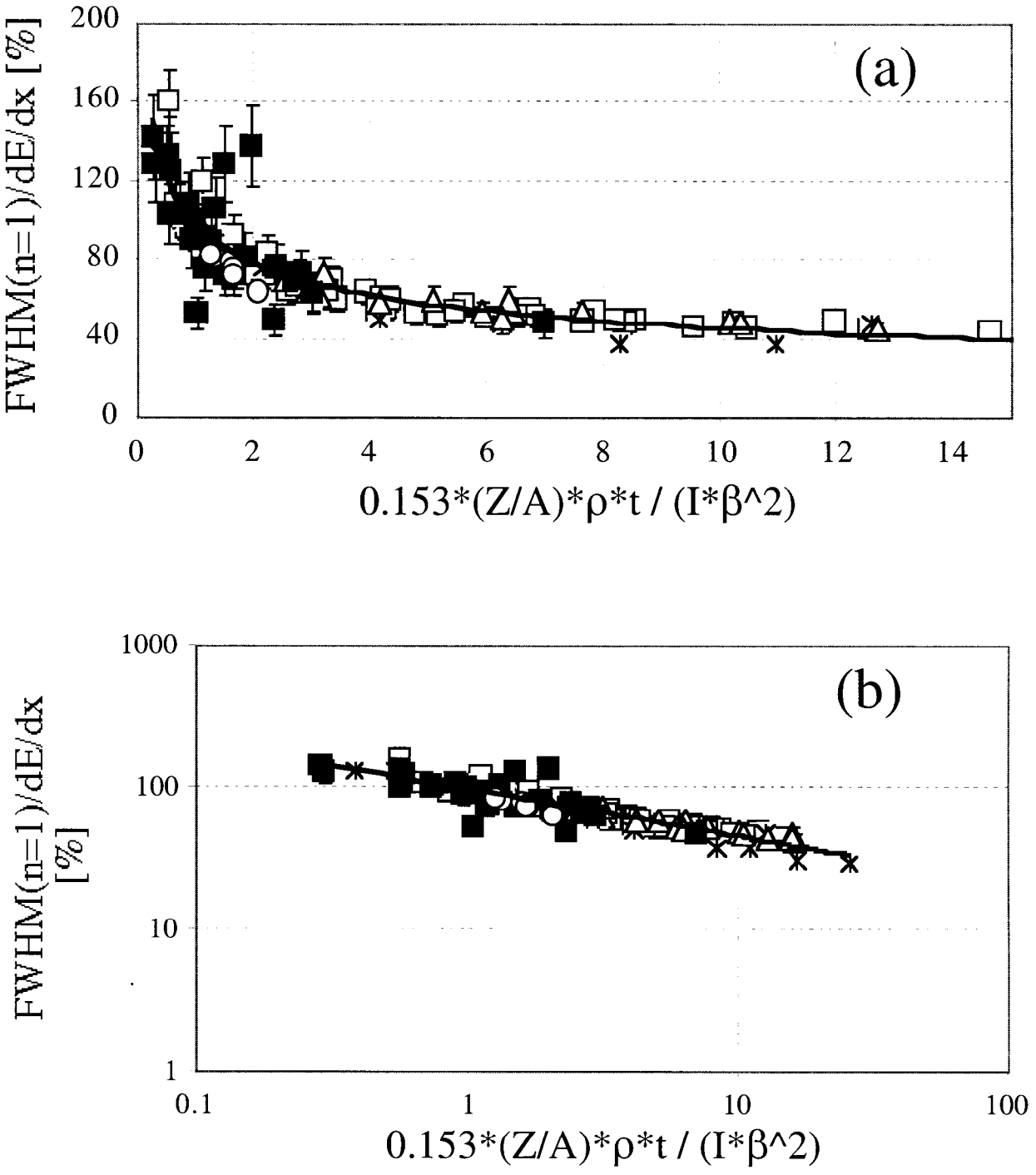

Figure 7: Author's compilation of FWHM(n=1) / dE/dx resolution measurements from large experiments and tests [9,10], plotted as a function of electron density of the medium, and using (a) linear and (b) logarithmic scales. The large open circles are Allison-Cobb calculation for He based gas mixtures. The data from the large experiments [9] are shown as black squares, all other data are from test results [10].

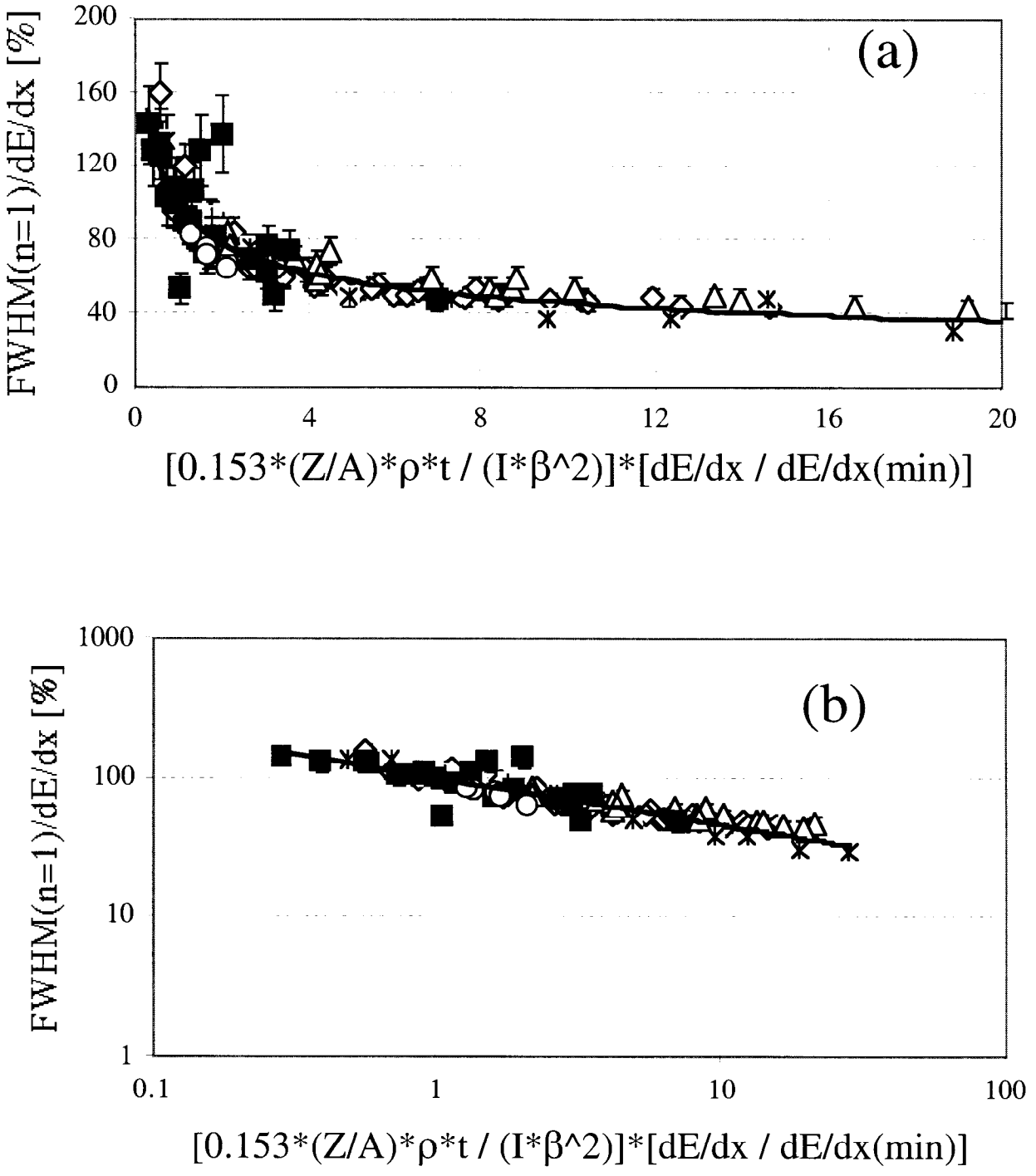

Figure 8: Author's compilation of FWHM(n=1) / dE/dx resolution measurements from large experiments and tests [9,10], plotted as a function of electron density of the medium, corrected for the relativistic rise, and using (a) linear and (b) logarithmic scales. The large open circles are Allison-Cobb calculation for He based gas mixtures. The data from the large experiments [9] are shown as black squares, all other data are from the test results [10].

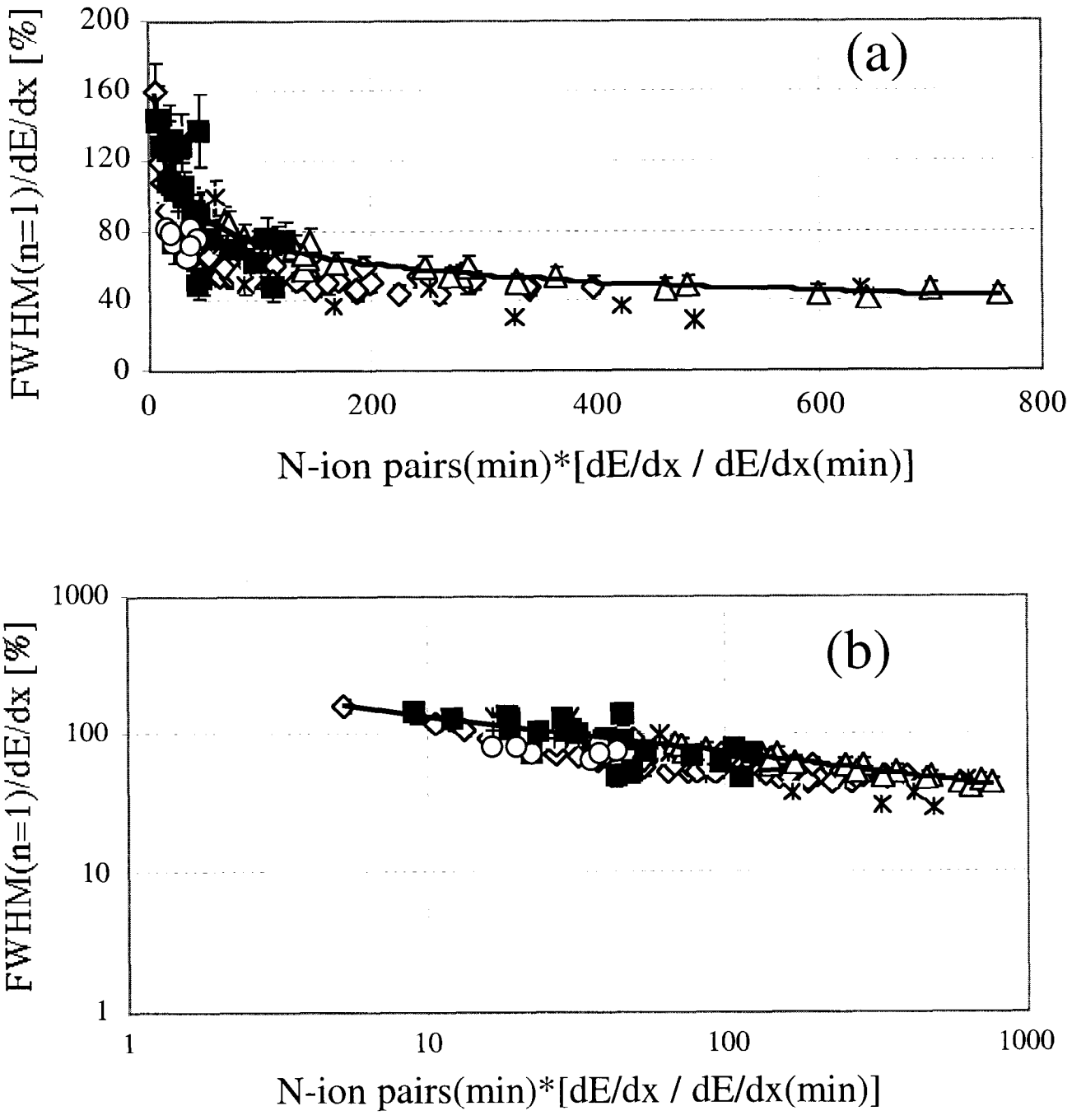

Figure 9: The author's compilation of FWHM(n=1)/dE/dx resolution measurements from large experiments and tests [9,10], plotted as a function of number of primary ions [11], on (a) linear scale and (b) logarithmic scale. The large open circles are Allison-Cobb calculation for He based gas mixtures. The data from the large experiments [9] are shown as black squares, all other data are from the test results [10]. The power law fit is done to the data of Lehraus [10].

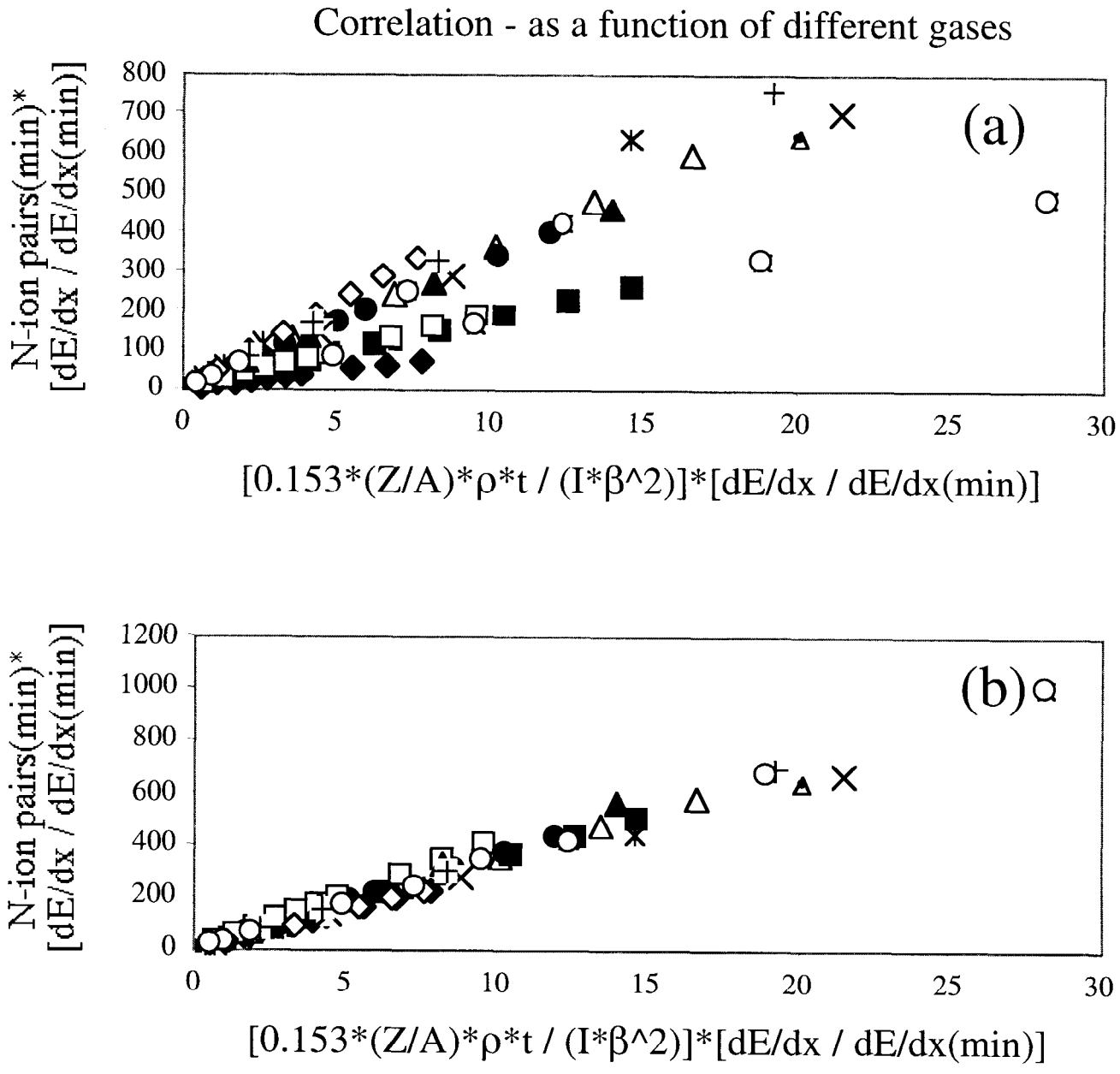

Figure 10: (a) Correlation for the x and y variables. Each slope corresponds to a different gas, while varying the pressure and sample size. Similar poor results are obtained if other sources of the primary ions are taken from Table 1. (b) The author's arbitrary tuning of the number of primary ions in He, Xe, CO_2, C_3H_8, and iC_4H_{10} gases, which improves the correlation.

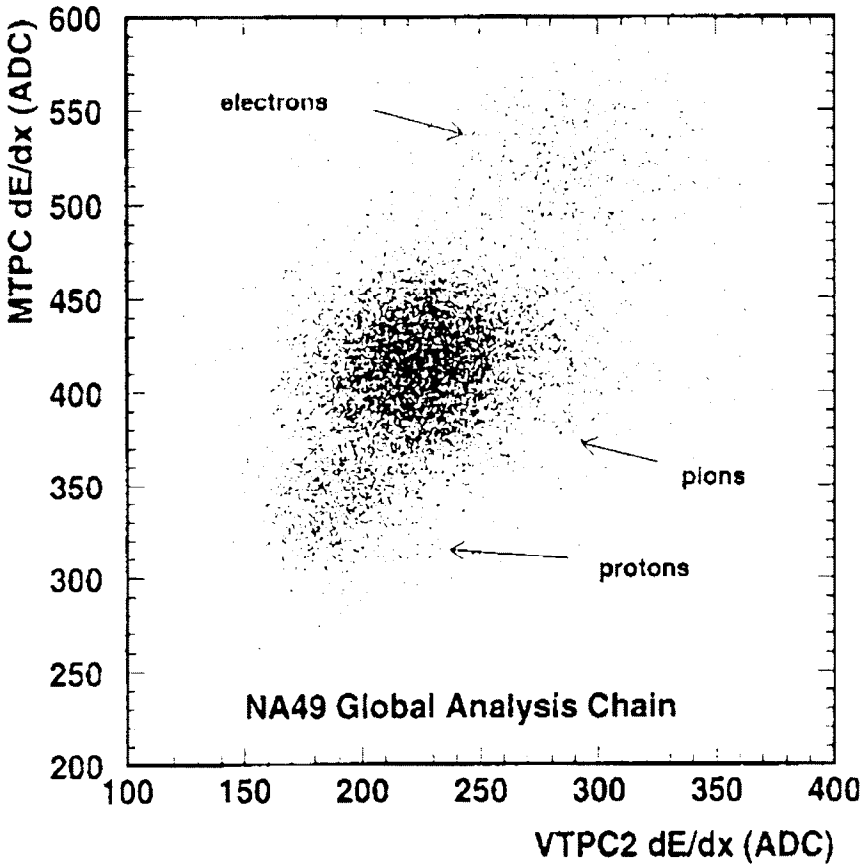

Figure 11: dE/dx particle identification in NA49, where up to 1500 tracks are recorded in one Pb-Pb collision..

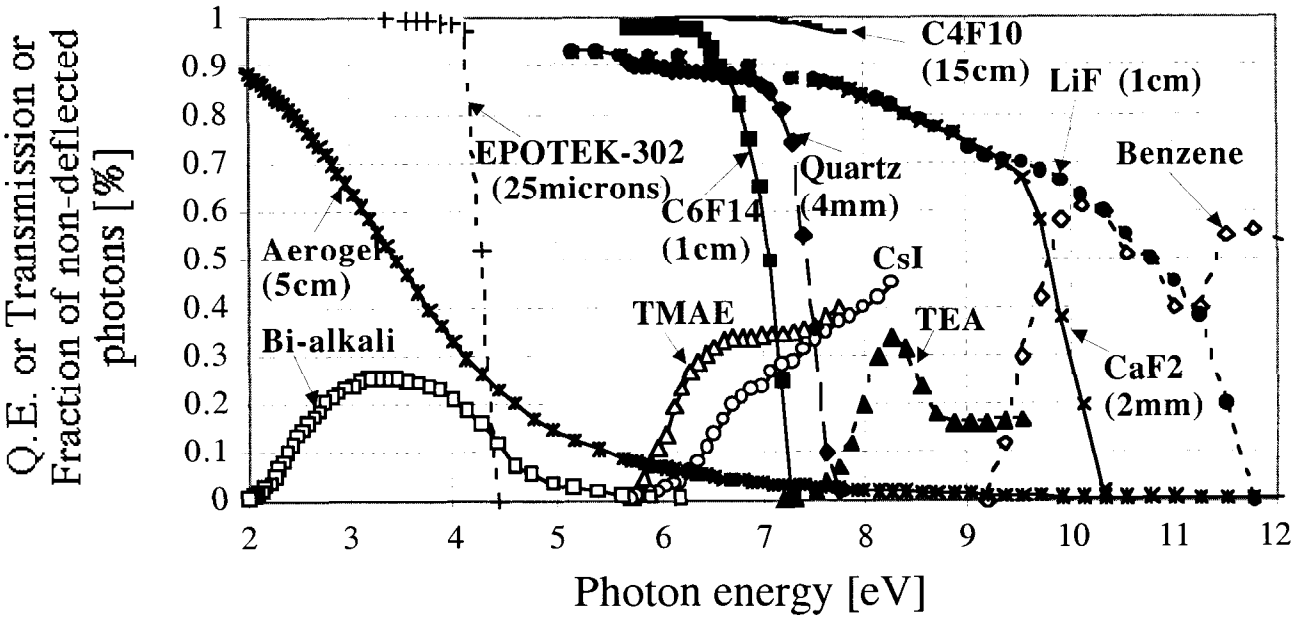

Figure 12: Examples of quantum efficiency, transmissions, and number of non-deflected photons (Aerogel only) for various RICH detector materials used in this paper by the author to estimate N_0 of various RICH detectors.

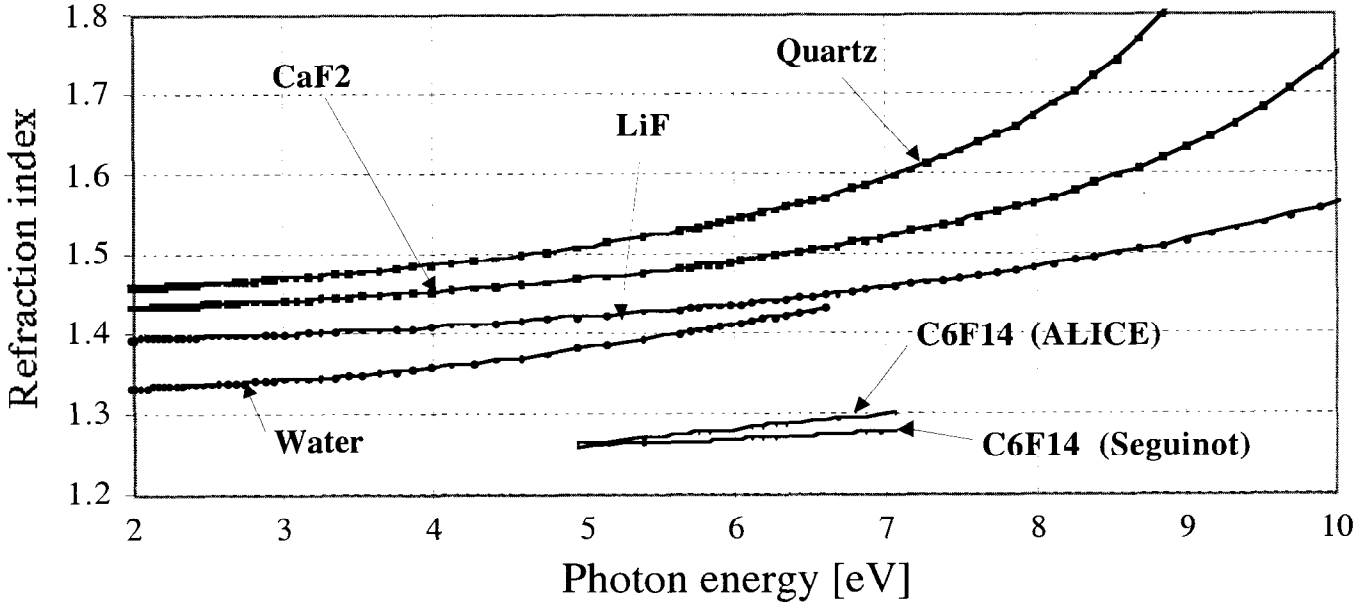

Figure 13: Examples of chromatic behavior of various radiator materials presented in this paper. The curves were calculated using fits to data presented in Ref. 19, except Alice C_6F_{14} results [39] and water [58].

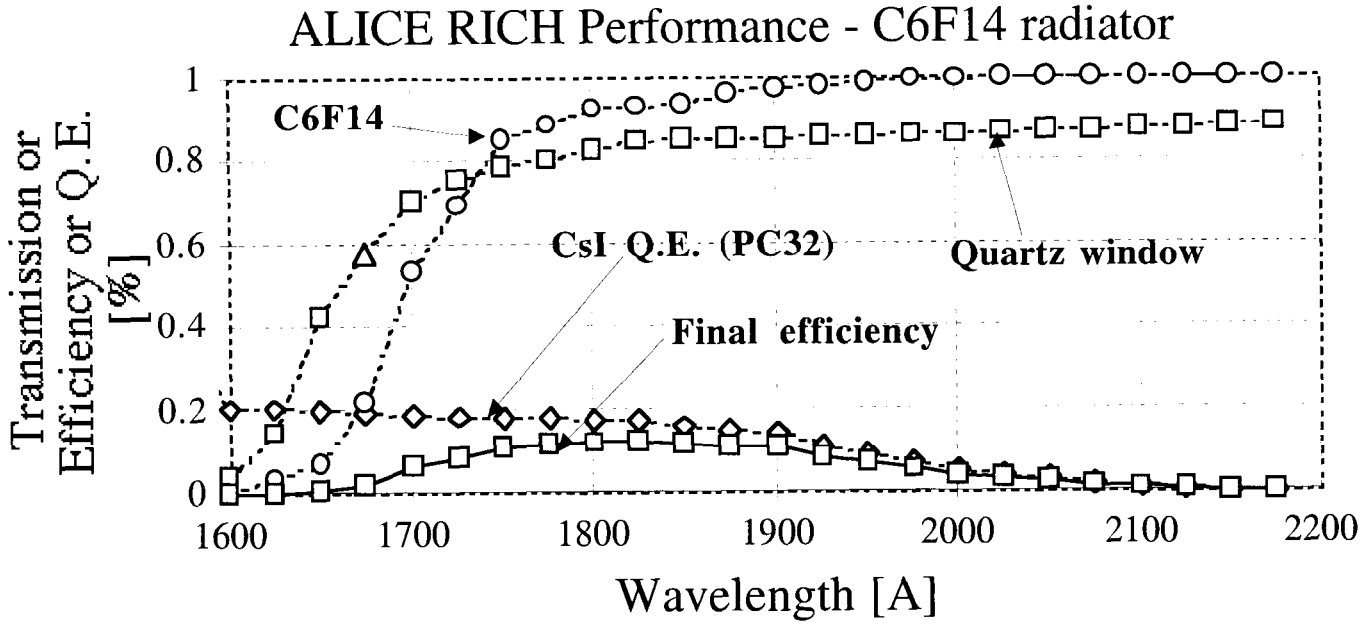

Figure 14: The CsI quantum efficiency in CH_4, and various transmissions in ALICE RICH for a track incidence of $\Theta_{inc}=0^o$. The final efficiency estimated by the author, yielding $N_{pe}\sim17$ (see Table 3).

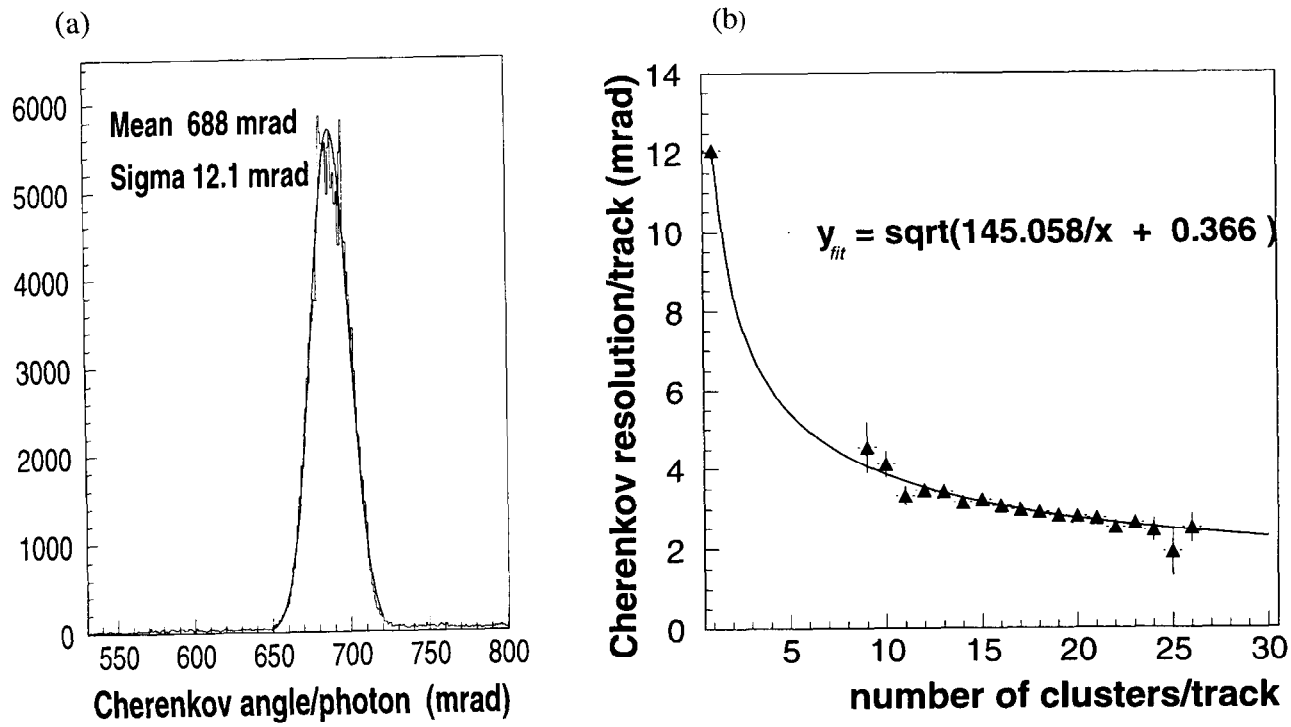

Figure 15: Measured Cherenkov angle resolution in ALICE RICH [39] with liquid C_6F_{14} radiator for a track incidence of $\Theta_{inc}=0^o$ and for (a) single photons, and (b) per track, and as a function of number of pad clusters (fit = $\sqrt{(12.04^2/Npe+0.605^2)}$). These are test beam results, which indicate a remarkably low background.

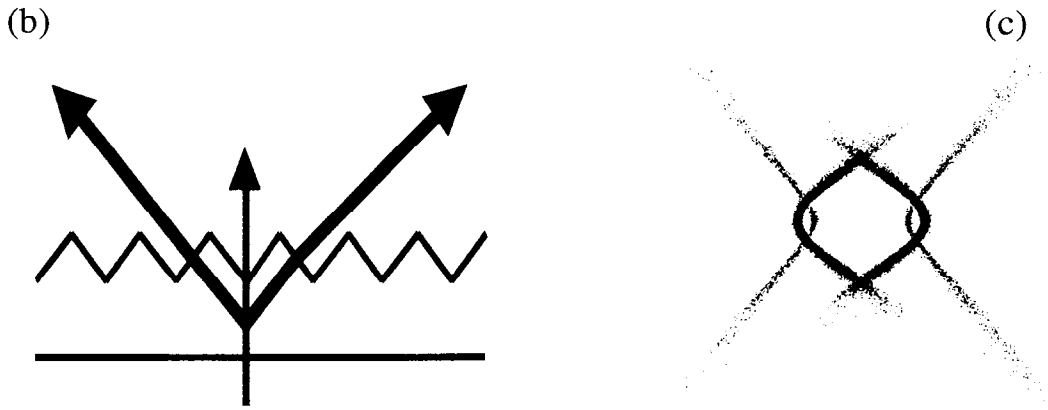

Figure 16: (a) CLEO RICH LiF radiator with grooves in the central detector region to prevent internal photon reflection, and (b) a rather complicated Cherenkov ring image resulting from a track incidence of $\Theta_{inc}=0^{o}$ [41].

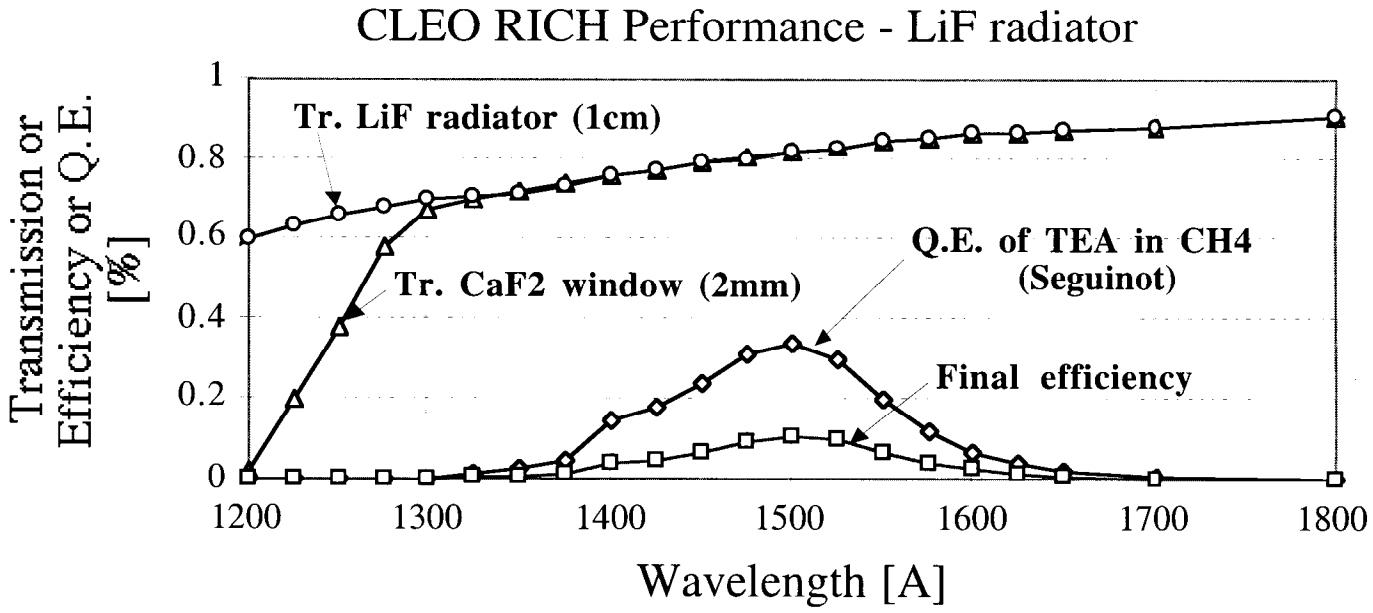

Figure 17: The TEA quantum efficiency in CH_4, and various transmissions in CLEO RICH for a track incidence of $\Theta_{inc}=0^{o}$. The final efficiency estimated by the author, yielding N_{pe}=18-19 (see Table 3).

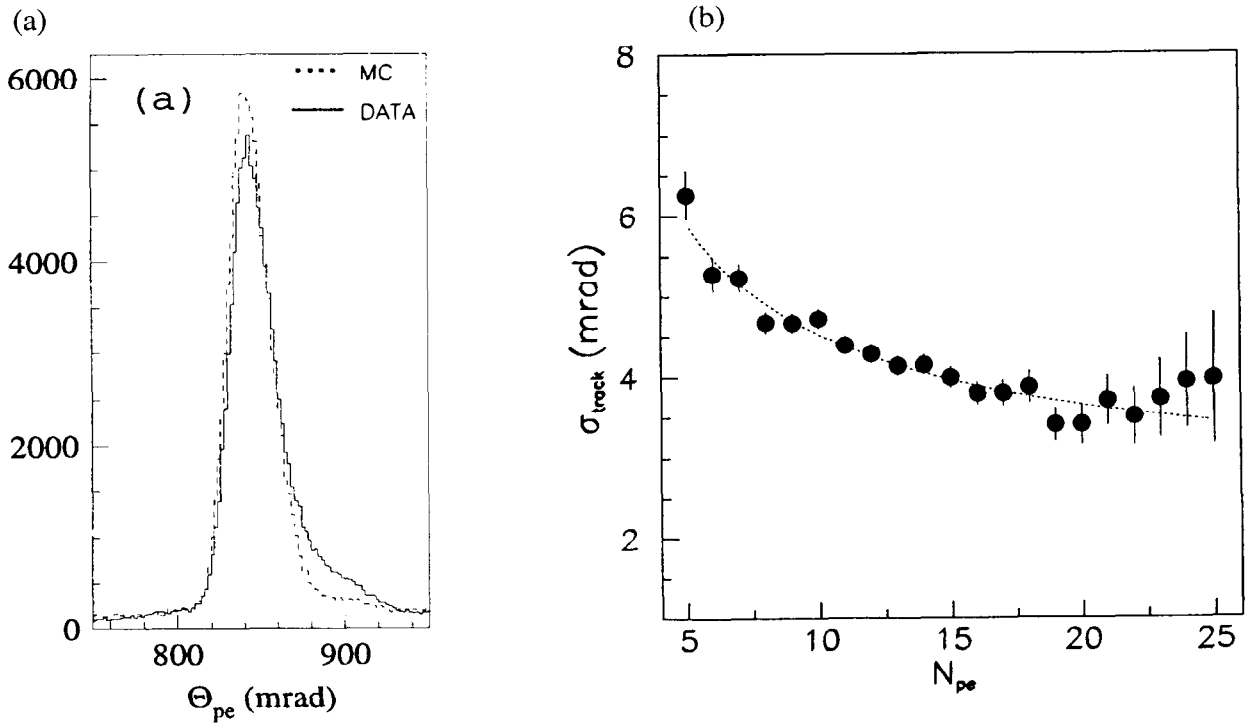

Figure 18: The Cherenkov angle resolution in CLEO RICH [41] with the saw-tooth LiF radiator for a track incidence of $\Theta_{inc}=0^{o}$, and for (a) a single photon (the distribution is not quite Gaussian), and (b) per track as a function of number photoelectrons (fit = $\sqrt{(11.7^2/Npe+2.43^2)}$. These are test beam results.

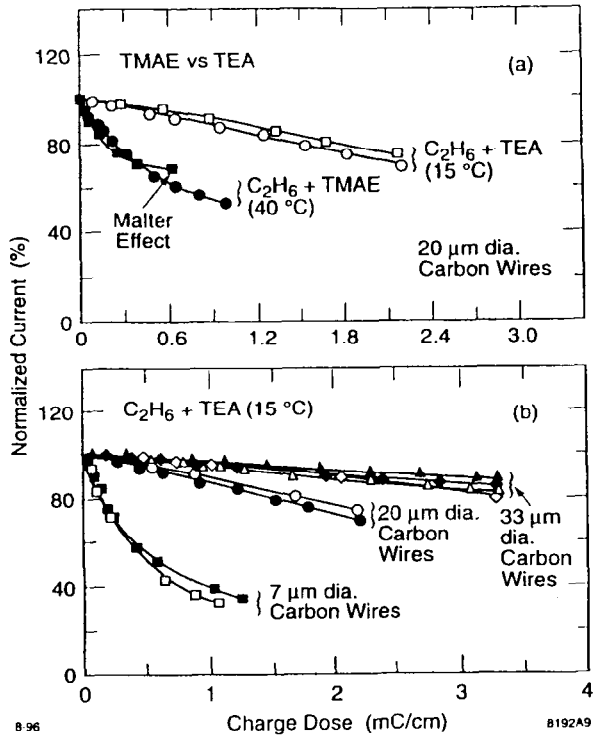

Figure 19. The anode wire ageing [42] in (a) TMAE vs.TEA, and (b) in TEA as a function of wire diameter (in both cases C_2H_6 is a carrier gas).

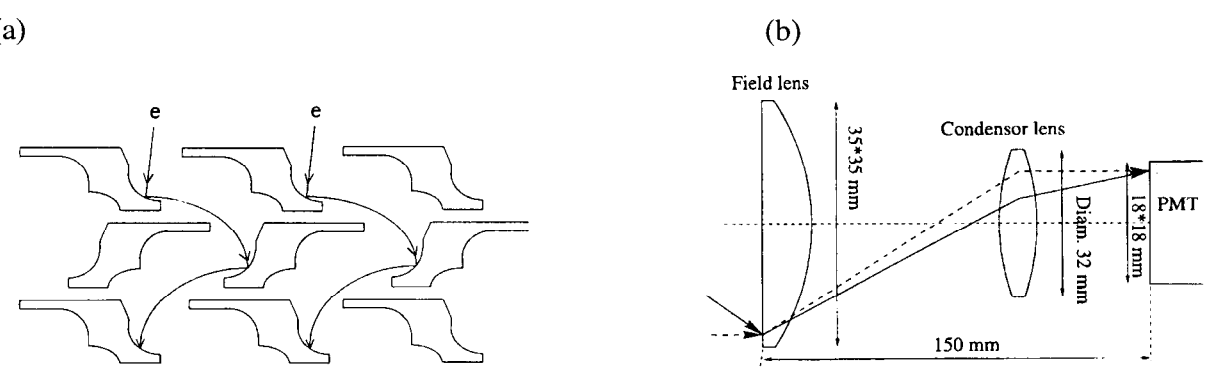

Figure 20: (a) A principle of the Hamamatsu multi-anode PMT is shown. Only ~75% of photoelectrons are transmitted in this structure. (b) A photon collection optics in front of each PMT has a transmission of only ~65% at 350nm [43].

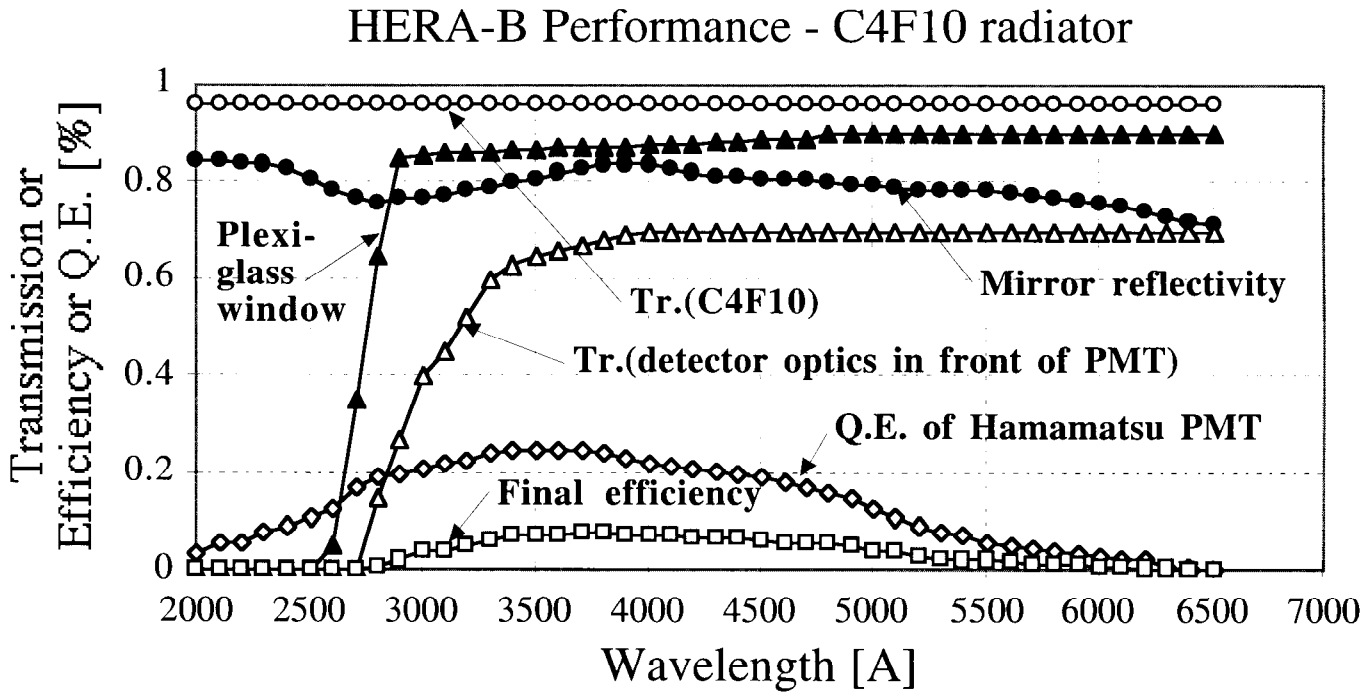

Figure 21: The PMT quantum efficiency and various transmissions in HERA-B RICH. The detector does not a full advantage of its potential due to a cut in the plexi-glass window and the detector optics. The final efficiency is estimated by the author, yielding N_{pe}~32 (see Table 3).

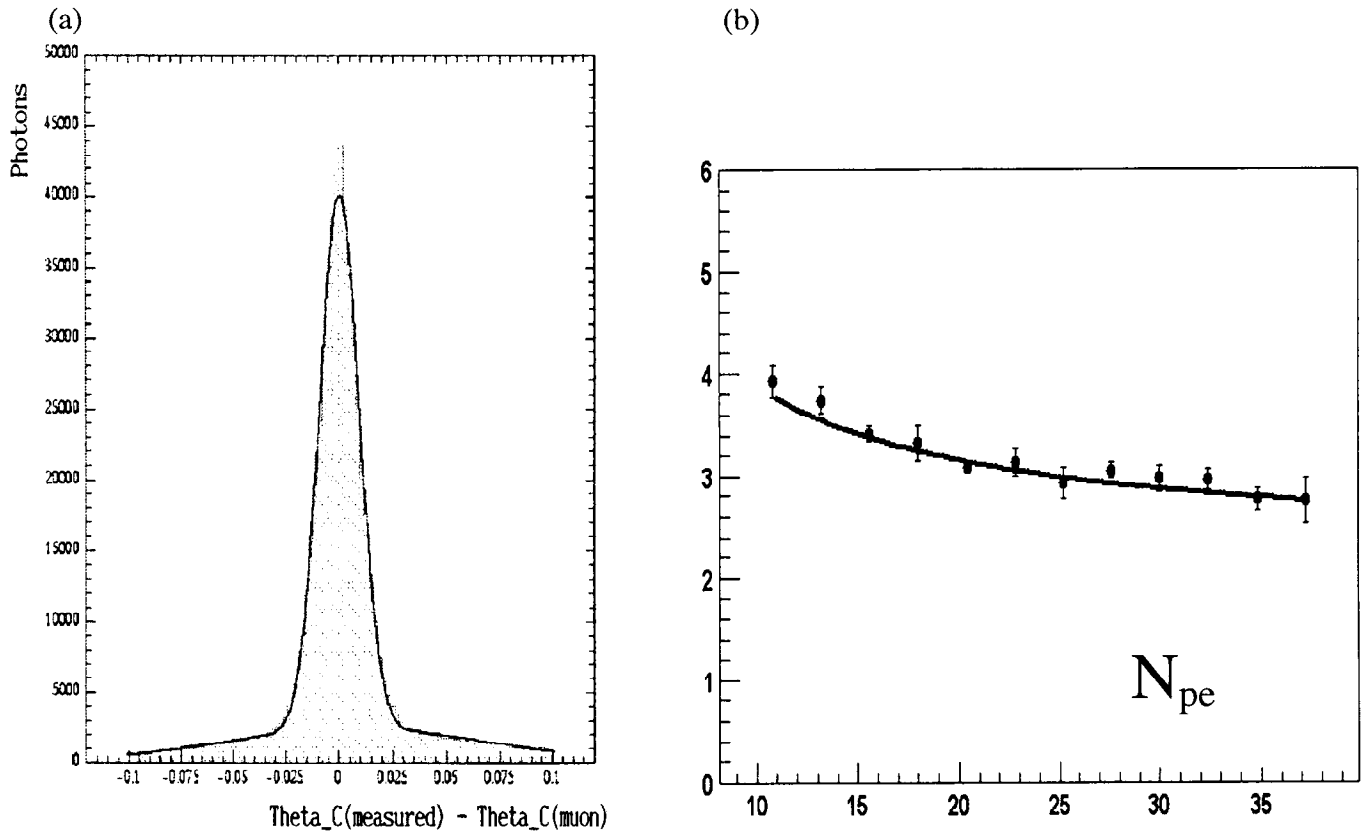

Figure 22: The Cherenkov angle resolution in DIRC RICH [44] is shown for (a) single photons from cosmic muons (9.3mrads). The background is larger than other RICH examples in this paper, and it is due to ambiguities, delta rays, showering, and possibly some scintillation in quartz (still under investigation). (b) Per track, and as a function of number photoelectrons in Bhabha events (preliminary result indicates a fit = $\sqrt{(10.02^2/Npe+2.2^2)}$.

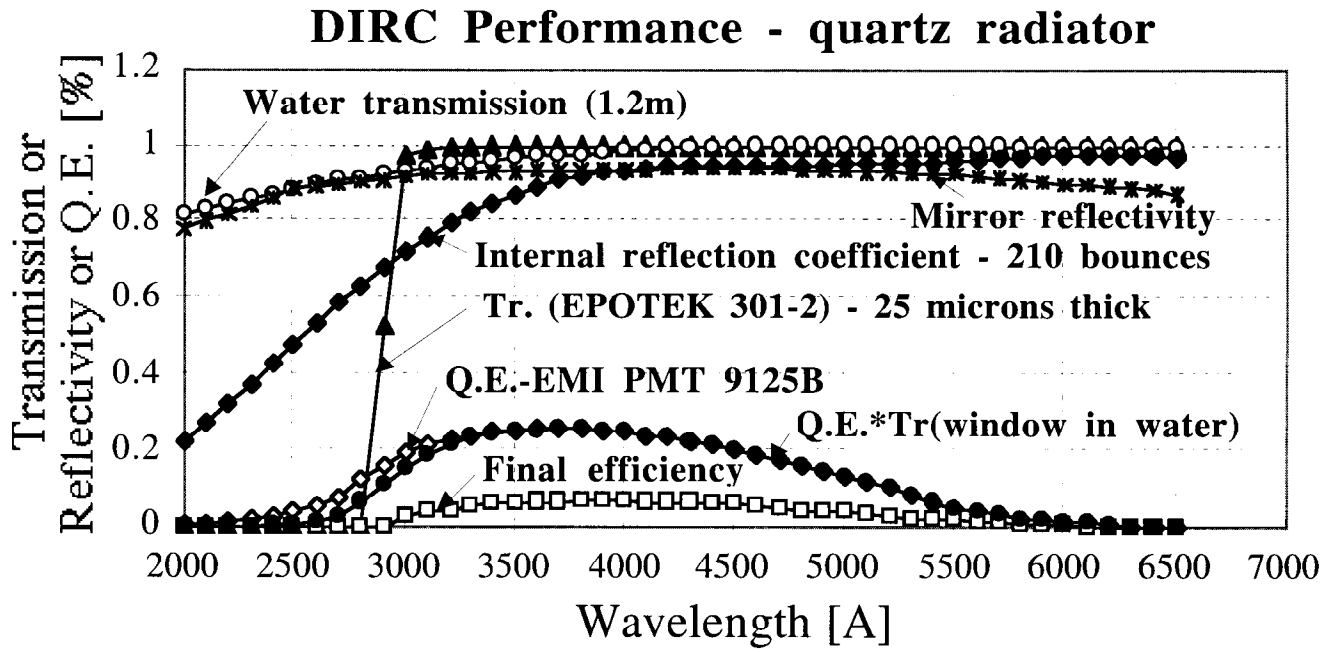

Figure 23: The EMI-9125 PMT quantum efficiency and various transmissions in DIRC RICH for a track incidence of $\Theta_{inc} = 0^o$ in the middle of BaBar active region. The DIRC bandwidth at the low wavelength is defined by the EPOTEK-301-2 optical glue, which is used to glue the quartz bars together. The efficiencies estimated by the author, yielding N_{pe}~32 (see Table 3).

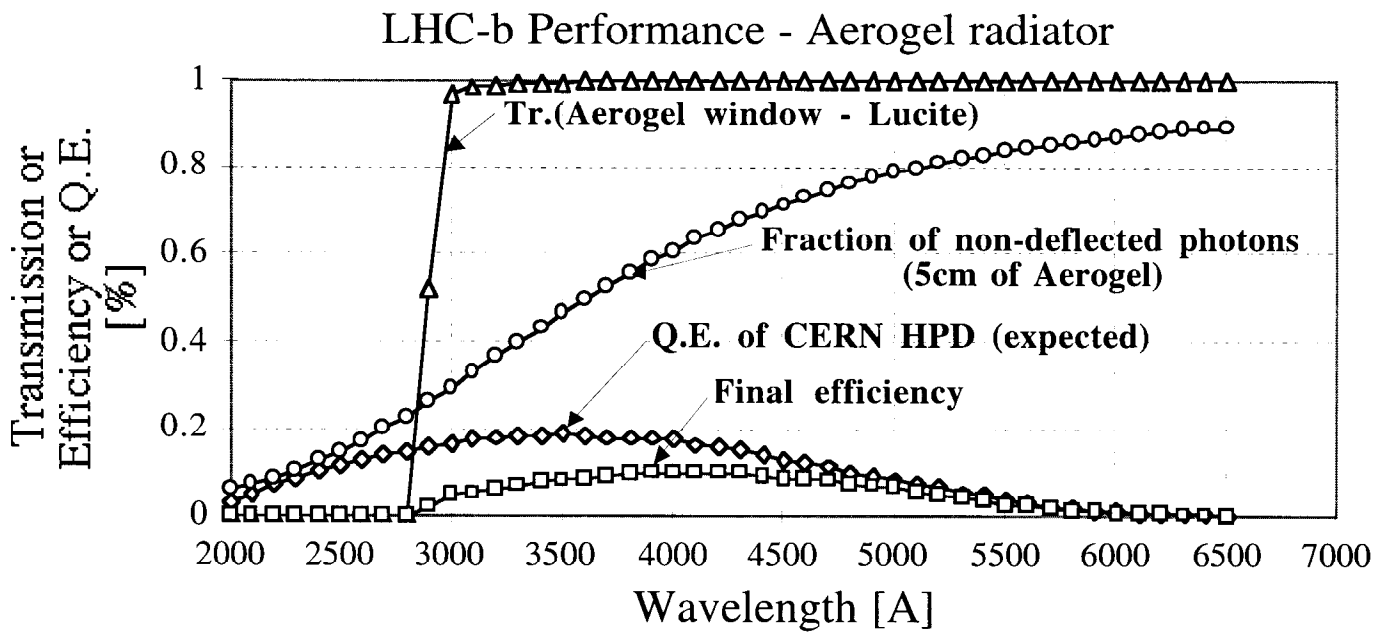

Figure 24: The HPD quantum efficiency and various transmissions in LHC-b RICH-1a with the aerogel radiator. The final efficiency is estimated by the author, yielding N_{pe}~16 for RICH-1a (see Table 3).

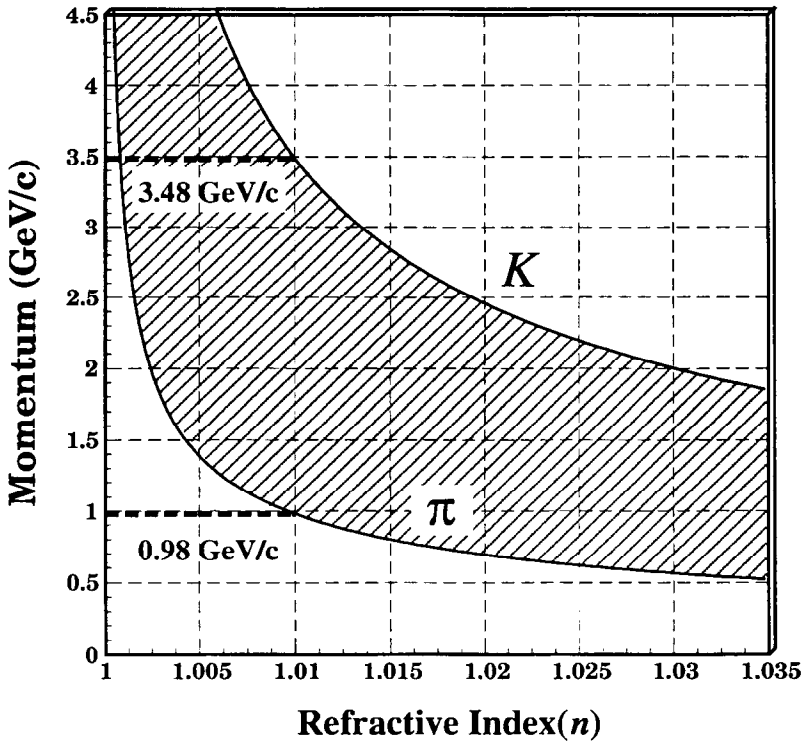

Figure 25: In the region above each curve (n β = 1), pions or kaons emit the Cherenkov light. The hatched area is the region where pions emit Cherenkov light and kaons do not [taken from Ref. 56].

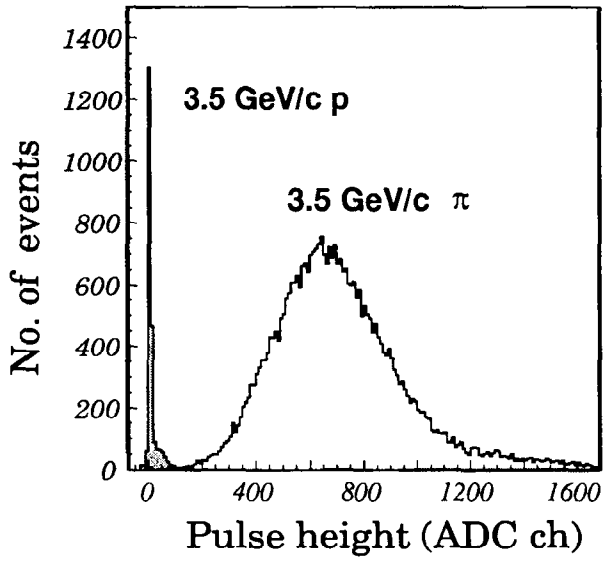

Figure 26: Pulse height spectra for 3.5 GeV/c pions (above threshold) and protons (below threshold) obtained by a single aerogel module, in which n = 1.015 silica aerogels were stacked [taken from Ref. 56].